

DNA-MGC+: A versatile codec for reliable and resource-efficient data storage on synthetic DNA

Ramy Khabbaz¹, Jérémy Mateos^{1,2}, Marc Antonini^{1,2}, and Serge Kas Hanna^{1,*}

¹Côte d'Azur University, CNRS, I3S, Sophia Antipolis, France

²Pearcode, Sophia Antipolis, France

*serge.kas-hanna@cncs.fr

ABSTRACT

The biochemical processes underlying DNA data storage, including synthesis, amplification, and sequencing, are inherently noisy. Consequently, base-level insertion, deletion, and substitution (IDS) errors, as well as sequence-level dropouts, occur and pose major challenges for reliable data retrieval. Here we introduce DNA-MGC+, a DNA storage codec designed to enable reliable and resource-efficient data retrieval under diverse operating conditions. We evaluate DNA-MGC+ across a wide range of *in silico* and *in vitro* settings, including experiments with both Illumina and Nanopore sequencing, and show that it consistently outperforms existing codecs. In particular, DNA-MGC+ achieves simultaneous gains in sequencing depth requirements, read cost, decoding time, storage density, and error-correction capability under explicit reliability constraints. Notable results include reliable decoding under IDS error rates of up to 24% in synthetic scenarios, and reliable retrieval at sequencing depths below 3× with read costs below 3.5 bits/nt under electrochemical synthesis for both Illumina and Nanopore sequencing.

Introduction

The exponential growth of digital information has made conventional storage technologies increasingly unsustainable¹, motivating research into alternative storage media, including the use of biological molecules. DNA has emerged as a particularly promising medium owing to its exceptional density and durability^{2,3}. One gram of DNA can theoretically store exabytes of data, and DNA molecules can remain stable for centuries at room temperature under suitable conditions^{2,3}, enabling compact and sustainable long-term storage. The DNA storage pipeline consists of a writing process, a storage phase, and a reading process. During writing, binary information is digitally encoded into quaternary sequences over the four DNA nucleotides Adenine (A), Guanine (G), Cytosine (C), and Thymine (T), which are then synthesized as short DNA molecules known as oligonucleotides. During reading, the stored oligonucleotides are amplified, sequenced, and the resulting reads are digitally processed and decoded to retrieve the original information.

While several proof-of-concept experiments have already demonstrated the feasibility of this pipeline, scalability remains a central challenge. The main obstacles are related to reliability, speed, and cost. DNA synthesis, amplification, and sequencing are inherently noisy biochemical processes that introduce *errors* and *biases* throughout the pipeline^{4,5}. Existing prototypes predominantly rely on high-fidelity synthesis and sequencing technologies to mitigate these effects. Such technologies, however, are slow and expensive, limiting current systems to small-scale demonstrations that store megabytes of data rather than the exabytes envisioned. A key step toward scalability is to address these errors and biases algorithmically rather than preventing them biochemically through high-fidelity technologies, thereby enabling the use of faster, cheaper, yet more error-prone technologies. Achieving this goal requires the development of efficient encoders and decoders (codecs) specifically adapted to the DNA storage channel, whose distinctive noise characteristics differ fundamentally from those encountered in conventional communication and storage systems⁴.

Errors in DNA storage manifest as insertion, deletion, and substitution (IDS) errors at the base level, affecting individual nucleotides⁴. In addition, biases introduced along the storage pipeline, such as those arising during PCR amplification, together with the stochastic nature of sequencing, can lead to sequence dropouts, i.e., the complete loss of encoded sequences⁵. A natural algorithmic approach to mitigate both errors and dropouts is the use of error-correcting codes (ECCs)^{6,7}. ECCs introduce structured logical redundancy into the stored data to enable reliable information retrieval under noisy conditions. A common design strategy is to employ a two-layer coding architecture in which the inner code adds redundancy within each encoded sequence to correct base-level errors, while the outer code introduces redundant sequences to compensate for dropout events⁸.

ECCs provide several key benefits that enhance DNA storage systems. First, they improve data retrieval reliability by reducing the probability of decoding failures in the presence of errors and dropouts⁹. Second, they reduce the number of sequencing reads required for successful decoding, which in turn decreases both the data retrieval time and the overall

sequencing effort¹⁰. Third, in addition to decreasing sequencing depth, ECCs also allow reducing the number of physical molecular copies required for reliable data retrieval, thereby enabling higher storage densities¹¹. Fourth, they enable the correction of synthesis errors that may appear systematically across reads and therefore cannot be mitigated simply by increasing sequencing depth¹². Finally, by compensating for the noise introduced by faster and lower-cost synthesis and sequencing technologies, ECCs help reduce the overall system cost.

Due to the established benefits of ECCs, the design of codecs for DNA storage with robust error-correction capabilities has been the subject of extensive research. The ECCs adopted in existing DNA storage codecs vary widely in scope. In particular, they differ in whether they are used for error detection or error correction, whether they address base-level errors and/or dropouts, and in the types of base-level errors they can handle. Existing designs include codecs that combine dropout recovery with error detection^{3,10,13–17}, codecs that jointly address dropouts and substitution errors^{18–21}, and codecs whose ECCs support dropout recovery together with correction of all three types of IDS errors^{12,22–24}. In addition to providing error-correction capabilities, most of these codecs are also designed to satisfy content-specific constraints on the encoded DNA sequences, typically including limits on homopolymer length and GC-content balancing, with some also avoiding specific sequence motifs²³. These constrained coding strategies follow the general principle of preventing or reducing errors and biases by avoiding sequence patterns believed to be problematic for the underlying biochemical processes. Some works focus exclusively on constrained coding and therefore design codecs without explicit ECCs^{2,25–27}, with some additionally considering thermodynamic constraints^{25,27}. A recent study suggests that embracing errors and addressing them through ECCs is more efficient than attempting to avoid them through constrained coding alone²⁸. Finally, alternative encoding strategies based on degenerate bases and composite DNA letters have also been explored^{29–31}.

In this work, we focus on DNA storage codecs based on the standard four-nucleotide alphabet and introduce a novel codec called DNA-MGC+ (Marker Guess & Check Plus). Through a broad range of *in silico* and *in vitro* settings, including varying error and bias profiles as well as experimental results obtained with both Illumina and Nanopore sequencing, we show that DNA-MGC+ consistently outperforms other codecs. The obtained results highlight the versatility of DNA-MGC+, demonstrating that its performance is not limited to a particular error profile or experimental workflow. Specifically, DNA-MGC+ achieves simultaneous gains across several key performance metrics under explicit reliability constraints, including the minimum required sequencing depth, read cost, decoding time, maximal error-correction capability, and storage density. Notable results include supporting reliable decoding under base-level error rates of up to 24% in synthetic scenarios, achieving an estimated storage density of 57 EB/g under experimentally derived error and bias profiles, and enabling reliable retrieval under both Illumina and Nanopore sequencing at sequencing depths below 3×, with associated read costs below 3.5 bits/nt. While most previous studies evaluate DNA storage codecs under high-fidelity workflows, typically involving material deposition-based synthesis (e.g., Twist Bioscience) and/or Illumina sequencing, our experimental validation also includes results combining electrochemical synthesis (GenScript) with Nanopore sequencing, both of which are substantially more error-prone than their conventional counterparts. These results show that, in addition to the performance gains achieved in typical workflows, DNA-MGC+ can also enable reliable storage in lower-fidelity and more error-prone settings, demonstrating its overall resource efficiency.

Our experimental study, which includes sequencing results with both Illumina and Nanopore, as well as constrained and unconstrained encoding variants of the same codec, reveals additional findings of broader and independent interest. In particular, we observe that comparable data retrieval performance can be achieved under both Illumina and Nanopore sequencing when using state-of-the-art Nanopore basecalling methods and efficient codecs. We also find similar data retrieval performance regardless of whether sequence constraints are imposed during encoding. Furthermore, we observe that less commonly considered constraints, such as thermodynamic properties related to free energy, have a more pronounced impact on data retrieval performance than commonly imposed constraints such as homopolymer length and GC-content balancing.

Results

Conceptual design of the DNA-MGC+ codec

We outline below the main steps of the DNA-MGC+ codec, describing how a binary file is encoded into a collection of DNA sequences and subsequently decoded from sequencing data. This high-level overview is intended to convey the structure and main operating principles of the codec, while the full mathematical and algorithmic details are deferred to the Methods section.

1. *Fragmentation*: The input binary file is partitioned into non-overlapping short fragments. The fragment length is determined as a function of the desired target DNA sequence length and user-defined codec parameters.
2. *Outer encoding*: The collection of binary fragments is encoded using a Reed–Solomon (RS) code³², which introduces *inter-sequence* redundancy by generating additional binary fragments. The RS code acts as an *outer code*, enabling recovery from dropouts (lost sequences) as well as correction of residual errors from other decoding stages.

3. *Indexing and inner encoding*: A unique binary index is appended to each fragment, after which the indexed fragments are encoded using the Marker Guess & Check Plus (MGC+) code^{33,34}. The MGC+ code acts as an *inner code* that introduces *intra-sequence* redundancy through structured encoding applied separately to each indexed fragment. This redundancy enables the correction of insertion, deletion, and substitution errors within individual DNA sequences. The MGC+ encoding process includes an unconstrained binary-to-quaternary mapping (00 ↔ A, 01 ↔ T, 10 ↔ C, 11 ↔ G) and therefore produces coded DNA sequences without content-specific constraints.
4. *Filtering*: The codec optionally supports filtering of the resulting DNA sequences based on *arbitrary* content-specific constraints. These may include, but are not limited to, homopolymer length, GC content, sequence motifs, or thermodynamic properties. This capability is enabled by the outer RS code, which allows the generation of an excess pool of candidate sequences from which any subset can be selected to represent the file.
5. *Decoding*: Decoding operates on noisy, unordered DNA sequences, which may correspond either to raw sequencing reads or to consensus sequences obtained after clustering. The sequences provided to the decoder are not required to match the reference sequence length, as insertions and deletions can be handled by the inner MGC+ code. Decoding proceeds by applying the inner MGC+ decoder, extracting fragment indices, decoding the outer RS code, and concatenating the recovered fragments to reconstruct the original file.

Overview of the evaluation framework

We evaluate the performance of the proposed DNA-MGC+ codec in comparison with existing codecs under three settings: (1) fully synthetic channel models, (2) experimentally derived *in silico* error and bias profiles, and (3) *in vitro* wet-lab experiments. In all settings, evaluation follows an end-to-end pipeline in which a binary input file is encoded into DNA sequences using the codec under consideration, processed through the associated channel model or experimental workflow, and decoded back into binary form.

In both *in silico* settings, the input consists of a randomly generated binary file of size 15 KB. We compare multiple variants of DNA-MGC+ against six representative DNA storage codecs: DNA-Aeon²³, HEDGES¹², DNA-Fountain¹⁰, DNA-RS^{19,20}, DNA-StairLoop²⁴, and an LDPC-based scheme¹⁸. These codecs were selected based on their prominence in the literature, the availability of wet-lab validation, and outcomes of previous benchmarking efforts¹¹. Across all codecs, we consider a total of 16 configurations spanning three code-rate classes with target rates of approximately 0.50 (low), 1.00 (medium), and 1.50 (high) bits per nucleotide (bits/nt). For all configurations in the *in silico* evaluations, the design length of the encoded DNA sequences is chosen to be as close as possible to 150 nucleotides. Codec parameters follow either the default settings provided by the original authors or configurations previously used for benchmarking in the literature¹¹. A complete specification of all configurations and parameters is provided in the Supplementary Information. Details of the *in vitro* experiment and the corresponding codec configurations are deferred to the dedicated sections describing the wet-lab experiment.

Performance is assessed using three metrics, reported consistently across all evaluation settings. First, decoding reliability is measured through the minimum *coverage depth* required to retrieve the file with an exact match, subject to a reliability constraint that requires successful decoding in 50 out of 50 independent trials. Second, we report the *read cost*, defined as the ratio of the minimum required coverage depth to the code rate. This metric is expressed in nucleotides per bit (nts/bit) and enables a fair comparison between codecs operating at different code rates by quantifying the minimum reading effort required per stored information bit. Third, we report the average *decoding time* measured at the minimum reliable coverage depth. Decoding time excludes clustering, alignment, and consensus formation, which are handled separately to isolate the computational cost of the codec decoding algorithms themselves. Unless otherwise stated, all results are obtained using a common preprocessing pipeline prior to decoding, in which noisy reads are clustered using CD-HIT³⁵, followed by multiple sequence alignment using Kalign³⁶ and consensus calling.

In silico performance under synthetic error and bias models

We start our performance analysis by evaluating the DNA-MGC+ codec in comparison with the other aforementioned codecs under a synthetic end-to-end channel model. This model captures key sources of variability in the DNA storage pipeline, including base-level errors, coverage bias across reference DNA sequences, and the stochastic nature of the sequencing process. The channel is parameterized by three independent quantities: a bias parameter, a coverage depth, and an error rate (Fig. 1a). Given a set of reference DNA sequences produced by the encoder, the channel generates a collection of noisy reads through three successive stages:

1. *Bias*: Each reference sequence is assigned a multiplicative weight drawn from a lognormal distribution with unit mean and standard deviation governed by the channel bias parameter. These weights are normalized to form a probability vector that defines the sequence-dependent sampling probabilities to be used in the next stage.

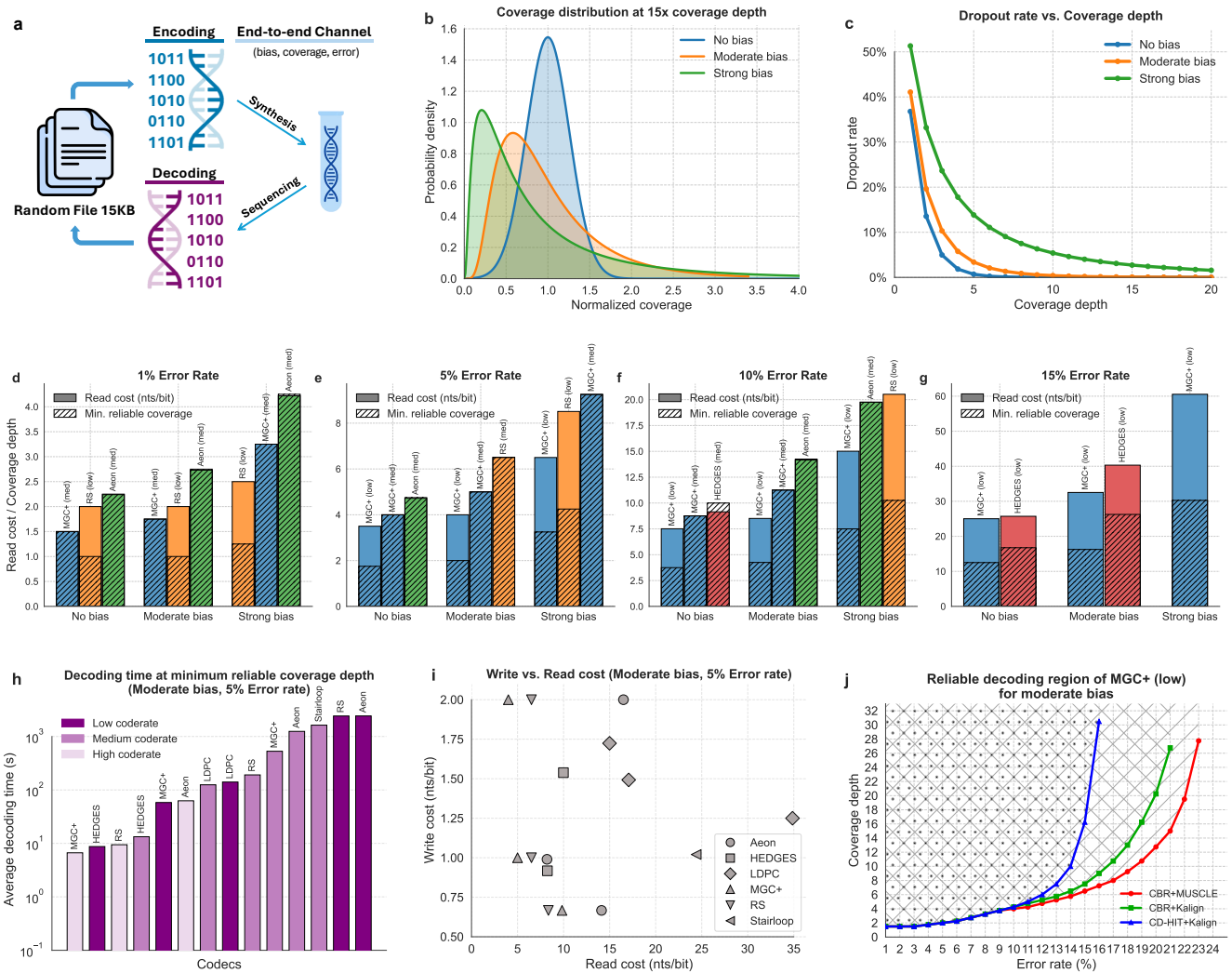


Figure 1. In silico performance of DNA-MGC+ and comparison codecs under synthetic error and bias models.

(a) Schematic of the evaluation pipeline, in which a random 15-KB file is encoded into DNA sequences and decoded after processing through a synthetic channel modeling the end-to-end DNA storage process, parameterized by bias, coverage depth, and error rate. (b) Coverage distributions for the three considered bias regimes, based on a lognormal model with unit mean and standard deviations $\sigma = 0$ (no bias), $\sigma = 0.5$ (moderate bias), and $\sigma = 1$ (strong bias). Coverage distributions are normalized by their mean, which equals the coverage depth, set to 15 \times in this plot. (c) Dropout rates as a function of coverage depth across the three bias regimes, showing the expected fraction of reference sequences receiving zero reads. (d)–(g) Minimum coverage depth and associated read cost achieved by the three best-performing codecs across the different bias and error combinations. (h) Average decoding times for the moderate bias and 5% error rate scenario, measured at the minimum coverage depth required for reliable decoding. (i) Trade-off between write cost and read cost for the moderate bias and 5% error rate scenario. (j) Reliable decoding region of the DNA-MGC+ codec (low-rate configuration) for the moderate-bias case, highlighting the error rate and coverage depth values for which reliable decoding is achievable under different clustering–alignment combinations.

- Coverage:** Reads are generated by random sampling with replacement according to the probability vector obtained in the previous stage, where the total number of reads is equal to the number of reference sequences multiplied by the channel coverage depth parameter.
- Error:** Base-level errors are introduced randomly and independently into each read according to the channel error rate, with substitutions, deletions, and insertions occurring in fixed proportions of 53%, 45%, and 2% of the total error rate, respectively, consistent with ratios reported in the literature⁵.

The coverage depth parameter fixes the average number of reads per reference sequence, while the bias parameter $\sigma \geq 0$ influences how unevenly these reads are distributed across sequences. The adopted bias model is motivated by experimental observations showing that the coverage distribution is positively skewed and is well-approximated by a lognormal distribution^{5,37}. In our simulations we consider three representative bias regimes: $\sigma = 0$ (no bias), $\sigma = 0.5$ (moderate bias), and $\sigma = 1$ (strong bias). When $\sigma = 0$, all sequences are sampled with equal probability, leading to a symmetric coverage distribution, whereas for $\sigma > 0$ the increasing standard deviation induces progressively skewed coverage distributions (see Fig. 1b). An important consequence of skewed coverage is an increased occurrence of sequence dropouts, whereby some reference sequences receive zero reads at the channel output. The dropout rate grows with increasing bias strength (see Fig. 1c).

Across the three bias regimes considered, we evaluate performance under four error rates (1%, 5%, 10%, and 15%), yielding a total of 12 synthetic channel scenarios with different (bias, error) combinations. For each scenario, we determine the minimum coverage depth required for reliable decoding for all 16 configurations of the comparison codecs, in addition to three configurations of DNA-MGC+ corresponding to target code rates of 0.50, 1.00, and 1.50 bits/nt. This is done by performing a binary search over coverage depths in the range [1, 32] with a resolution of 0.25, under the reliability constraint of 50 successful decodings (with an exact match) out of 50 trials. The corresponding read cost is then computed by normalizing the minimum coverage depth by the associated code rate. Figs. 1d–g report, for each of the 12 scenarios, the three best-performing codecs in terms of read cost, together with their corresponding coverage depths. The full numerical results for all performance metrics, covering all 19 codec configurations and 12 channel scenarios, are provided in Supplementary Tables S5–7.

The results in Figs. 1d–g show that the strongest performers across the synthetic channel conditions are DNA-MGC+, HEDGES, DNA-Aeon, and DNA-RS. In particular, DNA-MGC+ achieves the lowest read cost in 11 out of the 12 (bias, error) combinations, with the only exception occurring under the (strong bias, 1% error rate) scenario, where the low-rate configuration of DNA-RS attains a lower read cost. Beyond read cost, DNA-MGC+ also achieves the lowest coverage depth among all codecs for error rates of 5%, 10%, and 15% across all bias regimes, demonstrating that its reliability advantage persists as both dropouts and errors increase. Notably, under the highest error rate of 15%, only 2 out of the 19 tested codec configurations meet the reliability constraint within the simulated coverage depth range of [1, 32]. These two cases correspond to the low-rate configurations of HEDGES and DNA-MGC+ (see Fig. 1g). Both succeed in the no-bias and moderate-bias regimes, while DNA-MGC+ is the only codec that achieves reliable decoding under strong bias at 15% error rate.

In Figs. 1h–i, we highlight results for the (moderate bias, 5% error rate) scenario in terms of average decoding time and the relation between write cost and read cost. The average decoding times reported in Fig. 1h are measured at the minimum coverage depth required by each codec for reliable decoding, on a machine equipped with an AMD Ryzen™ Threadripper™ PRO 7985WX CPU, using a single CPU core and 256 GB of available memory. The results show that DNA-MGC+ is consistently among the three fastest codecs across all three code-rate classes. Fig. 1i illustrates the trade-off between write cost and read cost for the same scenario, where the write cost is defined as the reciprocal of the code rate expressed in nts/bit. Codecs with lower write cost (that is, higher code rate) generally require higher read cost to achieve reliable decoding, reflecting the classical tradeoff between logical redundancy added during encoding and redundancy supplied through coverage depth. DNA-MGC+ achieves a favorable balance in this tradeoff, as it lies near the lower envelope of the cloud of points, combining relatively low write cost with some of the lowest read costs among the tested codecs.

We further examined the robustness of the low-rate configuration of DNA-MGC+, which, as shown in Fig. 1g, supports reliable decoding at error rates up to 15% even under strong bias. Building on this observation, we assessed how far the error rate can be increased while still satisfying the reliable decoding constraint within the coverage depth range of [1, 32]. Using the same preprocessing pipeline applied across all codecs (CD-HIT + Kalign), we found that reliable decoding remains achievable up to an error rate of 16% under moderate bias. Fig. 1j shows the reliable decoding region for the moderate-bias regime. Similar figures for the no-bias and strong-bias regimes are provided in Supplementary Figs. S1 and S2, showing that the maximum achievable error rate is also 16% in the no-bias case, and 15% in the strong-bias case. Our analysis further reveals that at these high error rates, clustering becomes the limiting factor as most reads end up being unclustered. This in turn renders the subsequent alignment stage ineffective since the majority of clusters contain only a single read. Adjusting the parameters of CD-HIT did not help mitigate this effect.

To address the clustering bottleneck, we tested an alternative clustering algorithm introduced by Rashtchian et al.³⁸, referred to here as “Clustering Billions of Reads” (CBR), combined with the same alignment method Kalign. This approach extends the reliable decoding region to 21% under moderate bias, as illustrated in Fig. 1j. For error rates of 10% or less, CBR offers no measurable advantage over CD-HIT, and the improvement becomes apparent only as the error rate approaches the regime where CD-HIT no longer clusters effectively. We also tested pairing CBR with a more computationally intensive alignment algorithm, MUSCLE³⁹, which further extends the reliable decoding region to 23% under moderate bias. Beyond this point, even CBR becomes ineffective as almost all reads remain unclustered. For the no-bias and strong-bias regimes, the results provided in Supplementary Figs. S1 and S2 indicate that by using CBR and MUSCLE, DNA-MGC+ achieves reliable decoding up to an error rate of 24% in the no-bias case, and 21% in the strong-bias case.

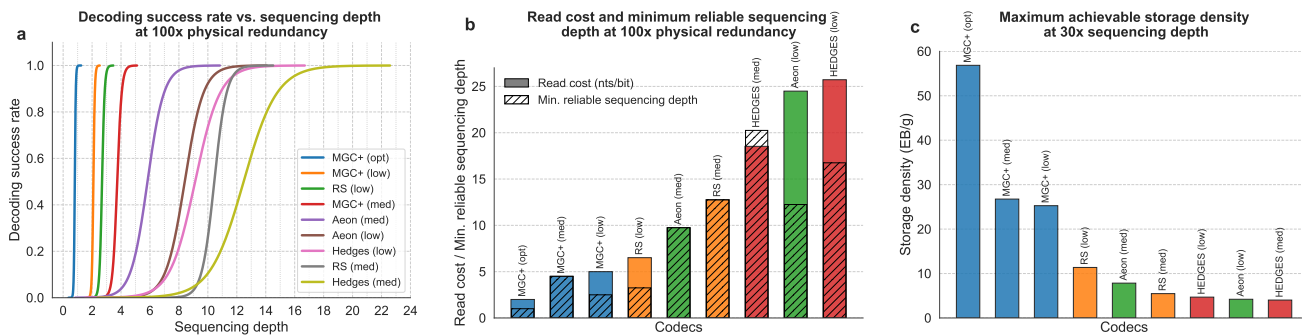


Figure 2. In silico performance of DNA-MGC+ and comparison codecs under experimentally derived error and bias profiles. (a) Decoding success rate as a function of sequencing depth at a fixed physical redundancy of 100× under the DT4DDS low-fidelity workflow. Solid curves correspond to logistic regression fits of the empirical decoding outcomes. (b) Minimum sequencing depth required for reliable decoding at 100× physical redundancy, together with the corresponding read cost. (c) Maximum achievable storage density, expressed in exabytes per gram of DNA, at a fixed sequencing depth of 30×, computed from the minimum physical redundancy required for reliable decoding.

In silico performance under experimentally derived error and bias profiles

Our second *in silico* performance evaluation follows a standardized workflow based on DT4DDS⁵, a digital twin for DNA data storage built on real experimental datasets and designed to reproduce the behavior of state-of-the-art storage pipelines. In this study, we focus on the “low-fidelity” workflow defined in Ref.¹¹, which models a pipeline consisting of electrochemical synthesis (e.g., GenScript), amplification using an error-prone polymerase (e.g., Taq), and short paired-end Illumina sequencing. This scenario is characterized by higher error rates and more pronounced bias compared with high-fidelity pipelines based on material deposition synthesis (e.g., Twist) and low-error polymerases (e.g., Q5). As such, it provides a particularly relevant setting for assessing the ability of the codecs to compensate for the error and bias introduced by low-fidelity technologies.

Compared with the synthetic model used previously, this experimentally derived model imposes a more nuanced error profile. While the overall error rate is fixed at approximately 1.5%, errors exhibit correlation across neighboring bases, position-dependent behavior with increased rates near sequence extremities, and asymmetric substitution patterns derived from empirical measurements. In addition, each stage of the workflow is modeled separately, such that the resulting error composition reflects the successive biochemical processes rather than a simple end-to-end mixture. For example, under the considered workflow, deletions predominantly originate during synthesis, whereas substitutions mainly arise during sequencing.

The experimentally derived workflow also provides a more refined treatment of coverage. Instead of a single coverage depth parameter, the model enables separate parametrization of *physical redundancy* and *sequencing depth*. Physical redundancy is defined as the average number of physical DNA molecules per reference sequence during storage, whereas sequencing depth corresponds to the average number of sequencing reads obtained per encoded sequence. This distinction is important because physical redundancy directly constrains the achievable storage density (SD), which can be approximated as

$$SD \approx \frac{\text{code rate}}{\text{physical redundancy}} \times 113.7,$$

where the rate of the codec is expressed in bits/nt and the storage density in exabytes per gram of DNA (EB/g)¹¹. A codec that maintains reliable decoding at low physical redundancy therefore unlocks higher storage densities, since fewer molecular copies are required for data retrieval.

Using the low-fidelity workflow, we evaluate the same 19 codec configurations examined under the synthetic model on a randomly generated 15-KB file, together with an additional DNA-MGC+ configuration of code rate 0.50 bits/nt whose parametrization is optimized for this specific workflow. In the synthetic model evaluation, DNA-MGC+ was assessed using fixed parametrizations across 12 different error and bias conditions. In general, it is possible to optimize the parametrization of DNA-MGC+ according to the characteristics of the model under consideration. This corresponds to a design tradeoff between the redundancy allocated to the inner and outer codes, which we elaborate on in the Discussion section. The corresponding parameter settings for all evaluated configurations are provided in the Supplementary Information.

In one setting, we fix the physical redundancy to 100× and measure the decoding success rate as a function of sequencing depth (Fig. 2a), as well as the minimum sequencing depth and associated read cost required to satisfy the same 50-out-of-50 decoding reliability criterion used earlier (Fig. 2b). Notably, only 9 out of the 20 tested codec configurations meet the reliability

constraint within the simulated sequencing depth range of [1, 32]. Among these, the low-rate, medium-rate, and optimized DNA-MGC+ configurations achieve the lowest read costs. In particular, the optimized configuration enables reliable decoding at a sequencing depth as low as 1×, corresponding to a read cost of 2 nts/bit, while the two non-optimized DNA-MGC+ configurations also outperform all remaining codecs in terms of read cost. All numerical results for this setting are summarized in Supplementary Tables S8 and S9.

In another setting, we fix the sequencing depth to 30× and determine the minimum physical redundancy required for reliable decoding. While reduced physical redundancy, like reduced sequencing depth, increases the occurrence of sequence dropouts, it also introduces a more fundamental challenge: the limited number of physical molecular copies reduces variability across reads and limits the effectiveness of clustering (see Discussion section for more details). Fig. 2c reports the maximum achievable storage density (SD) for each codec configuration, obtained by applying the above SD formula using the measured minimum physical redundancy. The results show that the three DNA-MGC+ configurations achieve the highest storage densities, with the optimized DNA-MGC+ configuration enabling reliable decoding at a physical redundancy of only 1×, corresponding to a storage density of approximately 57 EB/g.

In vitro experimental evaluation

To evaluate the performance of DNA-MGC+ under *in vitro* experimental conditions, we encoded a file of size 24 KB¹ using four different configurations of DNA-MGC+ and one configuration of each of the comparison codecs DNA-Aeon and HEDGES. DNA oligonucleotides corresponding to the six codec configurations were synthesized in a single pool via electrochemical synthesis performed by GenScript. The target design length of the encoded DNA sequences was set to 126 nts, below the maximum length of 170 imposed by GenScript. This choice allowed sufficient margin for the inclusion of 20-nt forward and reverse primer sequences, as well as a 4-nt unique tag to distinguish among the six configurations. Sequencing was performed using both Oxford Nanopore sequencing and paired-end Illumina sequencing.

The four DNA-MGC+ configurations considered in this experimental evaluation are based on two distinct inner and outer code parametrizations with different redundancy levels. The first parametrization yields an overall code rate of 1.03 bits/nt and is denoted as design A, while the second introduces additional redundancy and results in a lower code rate of 0.71 bits/nt, denoted as design B. For each design, we consider an unfiltered variant, in which no constraints are imposed on the content of the encoded DNA sequences, as well as a filtered variant.

In the filtered variants, an excess number of candidate sequences is generated using the codec, and only those satisfying a set of constraints are retained. These constraints include restrictions on homopolymer length, GC content, and the avoidance of selected sequence motifs, together with an additional filtering step based on thermodynamic properties (Gibbs free energy). By design of the DNA-MGC+ codec, the filtering step does not affect the code rate, so the filtered variants of designs A and B retain code rates of 1.03 and 0.71 bits/nt, respectively. These constraints, however, do impact encoding and decoding complexity. Full details of the filtering criteria and parameter selection are provided in the Methods section and in Supplementary Table S1.

In addition to DNA-MGC+, one configuration of each of DNA-Aeon and HEDGES was included in the same experimental pool, with code rates of 1.0 and 0.61 bits/nt, respectively. These codecs were selected based on their performance in the *in silico* evaluations (Figs. 1 and 2), where both achieved reliable decoding and consistently ranked among the strongest performers behind DNA-MGC+. In particular, DNA-Aeon (1.0 bit/nt) was chosen for its favorable read cost performance at medium rate across multiple *in silico* scenarios (see Figs. 1d–g and Fig. 2b). HEDGES (0.61 bits/nt), on the other hand, was selected for its strong robustness to IDS errors at low rate (see Fig. 1g). Although DNA-RS also exhibited competitive *in silico* performance, its main advantage lies in the outer RS code, whose benefits are shared with DNA-MGC+ by design. At the inner code level, however, DNA-MGC+ provides stronger capabilities for correcting insertion and deletion errors. DNA-RS was therefore not included in the *in vitro* comparison, since its principal strengths are inherited by DNA-MGC+ and can be further enhanced through optimized redundancy allocation, as observed in Fig. 2.

The stored file was successfully decoded with an exact match under both Nanopore and Illumina sequencing, across all six codec configurations, albeit with quantitatively different performance outcomes. The performance comparison across multiple metrics is shown in Fig. 3. For each codec configuration, we report the minimum sequencing depth required for reliable decoding, determined via progressive read downsampling under the same 50-out-of-50 decoding reliability criterion used in the *in silico* evaluations. The corresponding read cost, expressed in nucleotides per information bit, is also reported. We further report the average decoding time for recovering the stored file, measured at the minimum sequencing depth required by each codec for reliable decoding. As in the previous results, decoding times exclude clustering, alignment, and consensus calling, which were performed using CD-HIT and Kalign.

For Nanopore sequencing, multiple Dorado⁴⁰ basecalling models were tested, revealing pronounced tradeoffs between basecalling accuracy and computational cost. The fast, high accuracy (hac), and super accuracy (sup) models exhibited basecalling runtimes differing by approximately one order of magnitude between successive models, with corresponding

¹The file is obtained by zlib compression of a text document containing the Universal Declaration of Human Rights in four different languages.

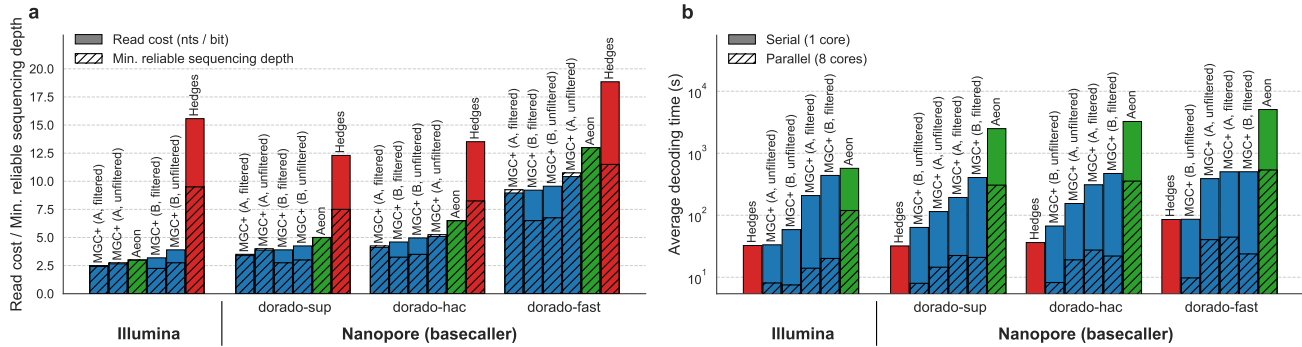


Figure 3. In vitro performance of DNA-MGC+ and comparison codecs under Illumina and Oxford Nanopore sequencing. (a) Minimum sequencing depth and corresponding read cost required for reliable decoding, obtained via progressive read downsampling, under Illumina and Nanopore sequencing. For Nanopore data, results are reported for multiple Dorado basecalling models with varying computational complexity. (b) Average decoding time required to recover the 24-KB stored file, measured at the minimum sequencing depth needed for reliable decoding for each codec configuration.

base-level error rates of $5.6 \pm 0.2\%$, $2.2 \pm 0.15\%$, and $1.4 \pm 0.1\%$ (averaged across the six codec configurations), respectively. As expected, the results in Fig. 3a show that reduced basecalling accuracy leads to a systematic increase in the minimum sequencing depth required for reliable decoding, and consequently in the associated read cost. Across all three basecallers, all four configurations of DNA-MGC+ consistently require lower sequencing depth and read cost than both DNA-Aeon and HEDGES. In particular, under the dorado-sup basecaller, the filtered variant of design B achieves the lowest minimum sequencing depth of 2.75 \times , while the filtered variant of design A attains the lowest read cost of 3.4 nts/bit. Furthermore, the filtered variants of DNA-MGC+ provide modest but consistent improvements over their unfiltered counterparts across all cases.

Under Illumina sequencing, we observed an average base-level error rate of $0.34 \pm 0.03\%$, which is lower than that of Nanopore sequencing, as expected. Overall, the performance trends under Illumina closely mirror those obtained with Nanopore. In particular, DNA-MGC+ outperforms both DNA-Aeon and HEDGES, with the filtered variant of design B achieving the lowest minimum sequencing depth of 2.25 \times , and the filtered variant of design A attaining the lowest read cost of 2.4 nts/bit. A comprehensive performance comparison across Nanopore and Illumina platforms is provided in the Discussion section.

In terms of decoding time, Fig. 3b reveals clear differences across codecs, with consistent trends observed under both Illumina and Nanopore sequencing. When decoding is performed on a single core, HEDGES achieves the fastest decoding time, with the unfiltered variant of design B of DNA-MGC+ following closely, while DNA-Aeon is approximately one order of magnitude slower. When parallelization across eight CPU cores is enabled, DNA-MGC+ achieves the fastest decoding performance overall, requiring less than 10 seconds on average for decoding. This improvement reflects the structure of the DNA-MGC+ decoder, which supports parallel processing at both the inner and outer code levels. The publicly available implementation of DNA-Aeon also supports parallel execution, and the corresponding parallel decoding results are therefore reported in Fig. 3b, whereas the available implementation of HEDGES does not support parallel decoding and is thus reported under single-core execution only. Another observation worth noting is that the unfiltered variants of DNA-MGC+ consistently decode faster than their filtered counterparts. This difference stems from the codec design, discussed in more detail in the Methods section, whereby filtered variants rely on a more complex decoding algorithm at the outer RS code level.

Discussion

The performance evaluations presented in this work demonstrate that DNA-MGC+ consistently outperforms existing codecs across a broad range of *in silico* frameworks and *in vitro* experimental conditions. These evaluations span different error and bias profiles as well as multiple sequencing technologies with distinct basecalling models, highlighting the *versatility* of DNA-MGC+ in delivering superior performance across diverse operating conditions. The *reliability* and *resource-efficiency* of DNA-MGC+ is reflected in several key performance metrics. Specifically, the codec achieves simultaneous gains in coverage depth requirements, read cost, decoding time, maximal error-correction capability, and storage density. In practice, these gains translate into improved data reliability, reduced sequencing effort, and faster data retrieval. Importantly, the results further indicate that DNA-MGC+ is efficient even under low-fidelity biochemical processes. Such processes are more cost-effective, and are therefore expected to play a central role in overcoming current scalability bottlenecks in DNA data storage in the future. These improvements are a direct consequence of the coding strategy implemented in DNA-MGC+, as discussed next.

The design of the DNA-MGC+ codec follows a two-layer architecture, in which logical redundancy is introduced at both

the inner and outer coding stages with complementary roles. At the inner level, an MGC+ code³⁴ protects against base-level errors by enabling the correction of insertions, deletions, and substitutions (IDS) within individual DNA sequences. At the outer level, a Reed-Solomon (RS) code³² mitigates the effects of coverage bias by enabling recovery from sequence dropouts, while also correcting residual errors that remain after inner decoding. Under a fixed target code rate, this separation of roles leads to a natural redundancy allocation tradeoff: allocating more redundancy to the inner layer than to the outer layer enhances IDS error-correction capability at the expense of reduced robustness to dropout events, and vice versa. When the underlying error and bias profile is known or estimated, this tradeoff can be optimized, as reflected by the improved performance of the optimized DNA-MGC+ configuration in Fig. 2.

Table 1. Inner and outer code components of selected codecs considered in this work, together with their scope of operation.

Codec	Inner code	Outer code	Inner code scope	Outer code scope
DNA-MGC+	MGC+	RS	IDS errors (correction)	Dropouts and residual errors
DNA-Aeon ²³	Arithmetic	Fountain	IDS errors (correction)	Dropouts
HEDGES ¹²	Hedges	RS	IDS errors (correction)	Dropouts and residual errors
DNA-Fountain ¹⁰	RS	Fountain	Substitution errors (detection)	Dropouts
DNA-RS ^{19,20}	RS	RS	Substitution errors (correction)	Dropouts and residual errors

Several of the comparison codecs considered in this work follow the same two-layer coding architecture as DNA-MGC+, including DNA-Aeon, HEDGES, DNA-Fountain, and DNA-RS, whose respective inner and outer components are summarized in Table 1. As observed in Figs. 1 and 2, codecs based on this inner-outer architecture generally achieve better performance compared to DNA-StairLoop²⁴ and the LDPC-based scheme¹⁸, which follow conceptually different design principles. DNA-Fountain is a notable exception, as its reduced performance stems from limitations of its inner code, whose functionality is deliberately restricted to detection rather than correction of substitution errors. The advantage of using an RS code as an outer code is well established in coding theory^{9,41}, as RS codes are optimal in recovering from sequence dropouts with minimal redundancy, while also allowing correction of residual errors after inner decoding. Consistent with this theory, DNA-RS and DNA-MGC+ consistently emerge as the strongest performers in bias-dominated regimes such as Fig. 1d and Fig. 2. In parallel, strong performance under high-error conditions is most evident for codecs whose inner codes support correction of IDS errors. This explains why DNA-MGC+, HEDGES, and DNA-Aeon outperform schemes limited to substitution-only correction in Figs. 1f–g. Overall, the gains of DNA-MGC+ with respect to existing designs arise from the combination of (i) enhanced IDS error-correction capability at the inner MGC+ layer; and (ii) the use of an outer RS code that is both optimal for mitigating sequence dropouts and capable of correcting residual inner-decoding errors.

The *in vitro* results in Fig. 3 further indicate how structural differences between codecs translate into distinct performance under Illumina and Nanopore sequencing. Achieving reliable decoding with limited reads is a dual challenge, as low coverage increases both sequence dropouts and the effective error rate in consensus sequences. Accordingly, the minimum sequencing depth required by a codec reflects both its outer-code robustness to dropouts and inner-code IDS correction capability. Notably, the results in Fig. 3 show that DNA-MGC+ maintains nearly identical sequencing depth requirements under Illumina and Nanopore (dorado-sup) sequencing, despite the higher base-level error rate of the latter. This stability is attributable to the strong IDS error-correction capability of the inner MGC+ code, which effectively compensates for elevated error rates and preserves overall decoding performance. In contrast, DNA-Aeon performs substantially better under Illumina and approaches the sequencing depth levels of DNA-MGC+, indicating comparable dropout robustness but weaker IDS correction capability. HEDGES exhibits similar performance across both platforms yet consistently requires higher sequencing depths than DNA-MGC+ and DNA-Aeon, suggesting that its primary limitation lies in dropout mitigation rather than in IDS correction.

Beyond the challenge of reliable decoding at low sequencing depths, the second studied *in silico* framework highlights a distinct and more stringent challenge: reliable decoding at low physical redundancy, which enables higher storage densities (Fig. 2c). While reduced sequencing depth limits the total number of reads, reduced physical redundancy limits the number of independent molecular copies of each reference sequence. Although both effects increase sequence dropouts, low physical redundancy introduces a more fundamental decoding challenge that cannot be resolved by simply increasing the number of reads. Specifically, when only a small number of physical copies of each DNA sequence are present, errors introduced during early stages of the storage pipeline, such as synthesis, tend to propagate across most subsequent reads corresponding to the same reference sequence. This results in reduced read variability and the emergence of systematic error patterns, which in turn limit the effectiveness of clustering and consensus calling. Consequently, a larger share of the error-correction burden must be handled by the codec itself rather than by upstream read-processing operations. The superior IDS error-correction capability of DNA-MGC+ at the inner-code level is reflected in the results shown in Fig. 2c, where reliable decoding is achieved at lower physical redundancies than comparison codecs, thereby enabling higher storage densities.

In addition to their role in dropout recovery and residual error correction, outer codes also influence the flexibility of

constrained coding strategies. For this reason, despite the aforementioned advantages of RS outer codes, Fountain-based outer codes have also attracted significant attention in the literature. A key feature of Fountain codes is their ability to generate a virtually unlimited number of encoded DNA sequences. This enables constrained coding through simple filtering, where sequences that violate the desired constraints are discarded until a sufficient number of valid sequences is obtained¹⁰. In the proposed DNA-MGC+ codec, we introduce a design methodology that allows this filtering paradigm to be extended to outer RS codes, as detailed in the Methods section. As a result, the DNA-MGC+ codec supports filtering based on arbitrary content-specific constraints while retaining the error-correction advantages of outer RS codes.

The *in vitro* results in Fig. 3a show that modest but consistent performance gains are achieved when filtering is applied to DNA-MGC+. The filtering used for this experiment imposes several concurrent constraints. These include limiting the maximum homopolymer length to four, enforcing a GC content between 45% and 55%, avoiding motifs such as di- and trinucleotide repeats, and ranking candidate sequences by their predicted folding Gibbs free energy (ΔG), with those whose ΔG values are closest to zero retained. The limited extent of the observed gains compared to the unfiltered case can be attributed to two main factors. First, the inherent robustness of DNA-MGC+ to errors and biases allows it to compensate for content-induced effects without the need to explicitly avoid them through constrained coding. Second, the impact of factors such as long homopolymers and high GC content on modern synthesis and sequencing technologies appears to be less detrimental than suggested in earlier works, which is in line with recent independent experimental findings²⁸.

Despite the limited magnitude of the gains, the consistent improvement observed with filtering indicates that some of the considered sequence properties do indeed influence the retrieval process. In particular, our statistical analysis of the experimental data reveals that ΔG is the dominant factor contributing to the observed gains. Specifically, we identify Spearman correlation coefficients of -0.31 for Nanopore and -0.26 for Illumina between $|\Delta G|$ of unfiltered DNA-MGC+ sequences and their sequencing read count, with p-values below 10^{-50} in both cases. These statistics support the hypothesis that sequences with ΔG closer to zero receive more reads and are therefore easier to decode. Additional details regarding the effect of ΔG on the overall coverage distribution are provided in Supplementary Note S3.

Methods

DNA-MGC+ codec design

Encoding. Consider an input binary file of size B bits. The DNA-MGC+ encoder outputs N reference DNA sequences that collectively represent the file, each of length L_{ref} nucleotides. The encoding is carried out through a series of structured transformations that introduce logical redundancy in order to enable reliable data retrieval under error and dropout events. This process, illustrated in Fig. 4, comprises the following sequential steps.

- (1) *Fragmentation:* The input binary file is partitioned into $K = \lceil B/k \rceil$ non-overlapping fragments, each of length k bits.
- (2) *Outer RS Code:* The K fragments are encoded using an outer Reed-Solomon (RS) code over the finite field $\mathbb{F}_{2^{\ell_{\text{out}}}}$ to introduce inter-sequence redundancy, where each RS symbol consists of ℓ_{out} bits. The outer RS code generates c_{out} redundant fragments, resulting in a total of $N = K + c_{\text{out}}$ encoded fragments.
- (3) *Indexing:* Each outer-encoded fragment is prepended with a unique binary index of length ℓ_{out} bits, forming indexed fragments of length $k + \ell_{\text{out}}$ bits.
- (4) *Inner MGC+ Code:* Each indexed fragment is individually encoded using the Marker Guess & Check Plus (MGC+) code to introduce intra-sequence redundancy. The encoding proceeds in two stages, where part of the redundancy is introduced in the binary domain, and another part is added in the DNA domain after binary-to-quaternary mapping.
 - (4.1) *Binary-domain redundancy:* The inner MGC+ code introduces $c_{\text{in}} + 1$ parity symbols derived from an underlying RS code over $\mathbb{F}_{2^{\ell_{\text{in}}}}$, where each RS symbol consists of ℓ_{in} bits. This adds $(c_{\text{in}} + 1)\ell_{\text{in}}$ redundant bits to each indexed fragment, resulting in binary sequences of total length $k + \ell_{\text{out}} + (c_{\text{in}} + 1)\ell_{\text{in}}$ bits. The first c_{in} parity symbols are referred to as *guess* parities, while the final parity symbol is referred to as the *check* parity, reflecting their distinct roles in the decoding procedure described later.
 - (4.2) *DNA-domain redundancy:* Each resulting binary sequence is mapped into a quaternary DNA sequence according to $00 \mapsto A$, $01 \mapsto T$, $10 \mapsto C$, and $11 \mapsto G$. Optionally, periodic 2-nt markers “AC” are inserted after every ℓ_{in} DNA symbols. The check parity symbol is further encoded by mapping it into a short DNA barcode of length β , where the used barcodes are drawn from a predefined DNA codebook with minimum edit distance d_{min} .

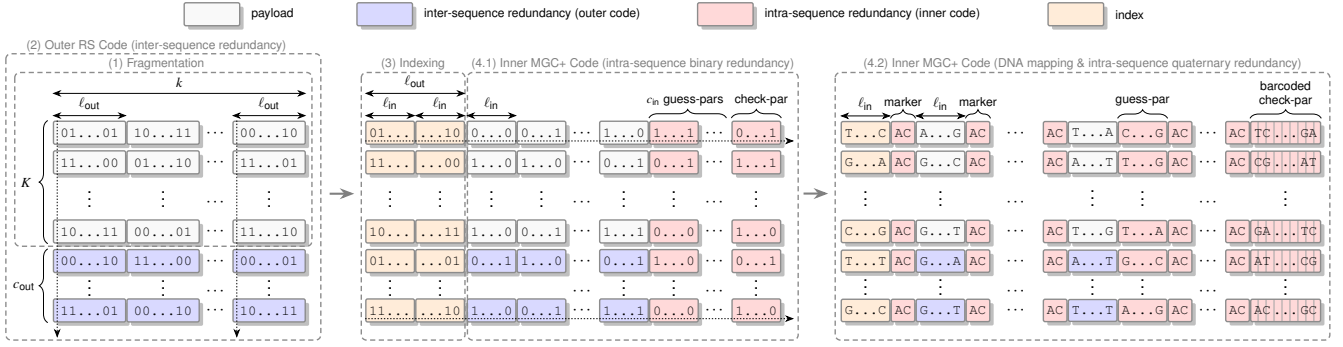


Figure 4. Schematic illustration of the DNA-MGC+ encoding process. (1) The input data is partitioned into K fragments, each of length k bits. (2) An outer Reed-Solomon code is applied across fragments to introduce inter-sequence redundancy, where each code symbol consists of ℓ_{out} bits, producing c_{out} additional sequences. (3) Each sequence is prepended with a unique binary index of length ℓ_{out} bits. (4.1) In the first stage of the inner MGC+ code, the indexed sequences are encoded to introduce binary intra-sequence redundancy, using symbols of ℓ_{in} bits and generating c_{in} guess parities in addition to a single check parity. (4.2) In the second stage of the inner MGC+ code, the resulting binary sequences are mapped to quaternary DNA sequences, followed by the insertion of periodic “AC” markers and further barcoding of the check parity.

The encoder therefore outputs a total of $N = K + c_{\text{out}}$ reference DNA sequences, where the length of each sequence is given by

$$L_{\text{ref}}(k) = \frac{1}{2} \left(\underbrace{k}_{\text{payload fragment}} + \underbrace{\ell_{\text{out}}}_{\text{index}} + \underbrace{c_{\text{in}} \ell_{\text{in}}}_{\text{guess-par}} \right) + 2 \left(\frac{k + c_{\text{in}}}{2\ell_{\text{in}}} + 1 \right) + \underbrace{\beta}_{\text{check-par barcode}}. \quad (1)$$

In summary, the DNA-MGC+ encoder is fully specified by the parameter set $(k, \ell_{\text{in}}, \ell_{\text{out}}, c_{\text{in}}, c_{\text{out}}, d_{\text{min}}, \beta, \text{marker mode})$, where k denotes the payload length of each fragment (in bits); ℓ_{in} and ℓ_{out} denote the symbol sizes (in bits) of the inner and outer codes; c_{in} is the number of guess parity symbols generated by the inner code; c_{out} is the number of redundant fragments generated by the outer code; d_{min} and β denote the minimum barcode edit distance and the corresponding barcode length used for encoding the check parity; and the marker mode specifies whether periodic DNA markers are inserted or not.

The fragment payload length k is a design parameter that is selected so that the reference DNA sequence length $L_{\text{ref}}(k)$ (see equation (1)) matches a target design length L_{target} as closely as possible. In general, the target length cannot always be matched exactly due to structural constraints imposed by the codec. For instance, since the inner and outer codes operate over symbols of length ℓ_{in} and ℓ_{out} bits, respectively, k must be divisible by both ℓ_{in} and ℓ_{out} . Moreover, the index length ℓ_{out} must also be divisible by ℓ_{in} since it is included in the inner code. In addition, when markers are used, the total number of inner code symbols (excluding the check parity) must be even to ensure periodicity. The underlying RS codes also impose the standard field size constraints of $2^{\ell_{\text{in}}} \geq (k + \ell_{\text{out}})/\ell_{\text{in}} + c_{\text{in}} + 1$ and $2^{\ell_{\text{out}}} \geq K + c_{\text{out}}$. The latter constraint is equivalent to $N \leq 2^{\ell_{\text{out}}}$, thereby limiting the total number of encoded DNA sequences to at most $2^{\ell_{\text{out}}}$ for a given file. Consequently, either ℓ_{out} must be chosen sufficiently large to enable the generation of enough sequences within a single encoding instance, or the input file must be partitioned into smaller independently encoded blocks, resulting in a multi-packet² representation.

Taking the aforementioned constraints into account, the fragment length k is selected as follows. Given a target design length L_{target} and fixed parameters $(\ell_{\text{in}}, \ell_{\text{out}}, c_{\text{in}}, c_{\text{out}}, d_{\text{min}}, \beta, \text{marker mode})$, the encoder determines k^* that minimizes $|L_{\text{ref}}(k) - L_{\text{target}}|$ subject to $L_{\text{ref}}(k) \leq L_{\text{target}}$. Thus, L_{target} serves as an upper bound on L_{ref} , and k^* minimizes the gap between the two. If an exact match is required, the remaining gap $L_{\text{target}} - L_{\text{ref}}(k^*)$ is filled with random DNA symbols. The encoding steps illustrated in Fig. 4 are applied once k^* is determined. If the input file size B is not divisible by k^* , random bits are added so that the final payload fragment has length exactly k^* . These padding bits are removed after decoding.

Throughout all results presented in this work, the following code parameters were fixed: $\ell_{\text{in}} = 8$, $\ell_{\text{out}} = 16$, $d_{\text{min}} = 5$, and $\beta = 12$. The different codec configurations of DNA-MGC+ were obtained by varying k , c_{in} , c_{out} , and the marker mode, with the full parameter specifications for each configuration provided in Supplementary Table S1. The code rate (in bits/nt) associated with each configuration follows from the ratio $B/(NL_{\text{ref}})$, where B is the input file size in bits, $N = K + c_{\text{out}}$ is the total number of encoded DNA sequences, and L_{ref} is the length in nucleotides of each sequence.

Filtering. The DNA-MGC+ codec supports filtering of the encoded DNA sequences according to arbitrary content-specific constraints prior to synthesis and storage. These constraints can be specified independently of the coding structure and may

²This approach requires additional metadata to ensure correct packet identification and reordering during decoding.

include limits on homopolymer length, bounds on GC content, exclusion of specific sequence motifs, or other biochemical and thermodynamic requirements. This capability is enabled by the outer RS code, which allows the encoder to generate an excess pool of candidate sequences from which any subset can be selected to represent the file. In particular, by setting the outer redundancy parameter c_{out} to its maximal value, the encoder can generate up to $N_{\text{max}} = 2^{\ell_{\text{out}}}$ candidate sequences. These candidate sequences are then screened, and a subset of $N \leq N_{\text{max}}$ sequences satisfying the desired constraints is retained for synthesis and storage, while the remaining sequences are discarded.

From a coding-theoretic perspective, this filtering step corresponds to a customized puncturing of the outer RS code, since certain codeword coordinates are deliberately omitted. In the unfiltered case, outer RS decoding is performed using the standard Berlekamp-Massey⁴² algorithm. When filtering is applied, decoding is carried out using the Welch-Berlekamp⁴³ algorithm, which is more suitable for punctured RS codes. Filtering does not affect the code rate $B/(NL_{\text{ref}})$ provided that N_{max} is sufficiently large to ensure the existence of at least N admissible sequences. The main cost of filtering lies in the increased decoding complexity, which is $O(N^3)$ under Welch-Berlekamp, compared to $O(N^2)$ under Berlekamp-Massey.

Decoding. The DNA-MGC+ decoder takes as input either noisy sequencing reads or, when applicable, consensus sequences obtained after clustering, and attempts to reconstruct the original binary file. A high-level description of the sequential decoding stages is provided below.

(1) *Inner MGC+ Code:* The inner MGC+ decoder processes each DNA sequence independently with the objective of correcting IDS errors and recovering the indexed binary fragments prior to outer decoding. Insertions and deletions induce symbol offsets, causing misalignment of the inner code symbol boundaries. The decoder therefore seeks to estimate an offset pattern, denoted by δ , reflecting the boundary shifts along the sequence. Given an estimate of this pattern, symbols affected by insertions or deletions are treated as erasures, while synchronized symbols are retained. In this manner, correction of IDS errors is reduced to erasure-and-substitution decoding over the underlying RS code.

(1.1) *DNA-domain processing:* The barcoded check parity is first decoded via minimum-distance decoding applied to the last β DNA symbols. If markers were introduced during encoding, an estimate of the offset pattern is then derived by solving a marker-centric maximum a posteriori (MAP) problem of the form $\hat{\delta} = \arg \max_{\delta} P(\delta \mid \text{marker observations})$, as detailed in Supplementary Note S1. The DNA symbols at the estimated marker locations are subsequently removed, and the remaining sequence is mapped to binary according to $A \mapsto 00$, $T \mapsto 01$, $C \mapsto 10$, and $G \mapsto 11$.

(1.2) *Binary-domain processing:* If an estimate $\hat{\delta}$ is available, the binary sequence is parsed accordingly. Symbols with nonzero estimated offsets are marked as erasures, while the remaining symbols are retained with their recovered values. All retained symbols, excluding the check parity, are then passed to the underlying RS decoder. The decoded fragment is subsequently validated using the check parity. If validation fails, a refined set of candidate offset patterns is generated and tested via a neighborhood search around $\hat{\delta}$, as described in Ref.³⁴. If none of the candidates yields a valid result, the entire sequence is declared an erasure, i.e., a dropout. If markers were not introduced during encoding and therefore no initial estimate $\hat{\delta}$ is available, candidate offset patterns are generated by exhaustive guessing and tested in turn, resulting in increased decoding complexity as discussed in Ref.^{33,44}.

(2) *Outer RS decoding:* Fragments declared as dropouts at the inner decoding stage are treated as erasures at the outer-code level, while incorrectly decoded fragments induce residual substitution errors that remain undetected. All recovered fragments are reordered according to their prepended indices, and outer RS decoding is then applied. Let E and S denote the numbers of erasures and substitution errors, respectively, among the N outer code symbols. Successful data retrieval with an exact match is guaranteed whenever $E + 2S \leq N - K$, which is equivalent to requiring that the number of correctly decoded fragments exceeds the number of incorrectly decoded fragments by at least K .

(3) *Defragmentation:* The recovered payload fragments are concatenated to reconstruct the original binary file.

Computational environment and software

All simulations and decoding experiments were conducted on a machine equipped with an AMD Ryzen™ Threadripper™ PRO 7985WX CPU and 256 GB RAM. The minimum required coverage (or sequencing) depth was determined via binary search over the interval [1, 32] with a resolution of 0.25, under the reliability constraint of 50-out-of-50 successful decodings with an exact file match. Reported decoding times correspond to the wall-clock time measured at the minimum coverage depth. Clustering, alignment, and consensus calling were excluded from decoding time measurements. All reported decoding times correspond to using a single CPU core, except for Fig. 3b, where results using 8 parallel CPU cores are also included.

Read clustering was performed using CD-HIT³⁵ (v4.8.1) or CBR³⁸, and multiple sequence alignment was carried out using Kalign³⁶ (v3.4.0) or MUSCLE³⁹ (v5.1), as specified for each experiment. For CD-HIT, the identity threshold and word size

were set to 0.80 and 5, respectively, with all other parameters left at their default values. For CBR, we used the implementation provided as part of the DNASTorageToolkit⁴⁵, modifying only the clustering diameter parameter to 50. To simulate the different codec configurations of DNA-Aeon, HEDGES, DNA-Fountain, and DNA-RS, we used the dt4dds-benchmark^{11,46} (v1.0.0) benchmarking suite. For DNA-Stairloop²⁴ and the LDPC-based scheme¹⁸, we used the respective GitHub repositories referenced in those works. For DNA-MGC+, we used our Python implementation, referenced in the Code Availability statement, requiring Python 3.9 or later and relying only on numpy (v1.21), scipy (v1.7), reedsolo (v1.5), and galois (v0.0.3).

The channel model used in the first *in silico* setting was implemented as part of this work and is included in the provided code. The second *in silico* setting is based on the DT4DDS⁵ digital twin framework and corresponds to the low-fidelity workflow described in Ref.¹¹. We used the implementation of this workflow provided in dt4dds-benchmark⁴⁶ (v1.0.0) as a black-box simulator to generate sequencing reads under specified physical redundancy and sequencing depth. For the wet-lab experiment, the primer sequences were generated using the DSP Tools software⁴⁷. The folding Gibbs free energy (ΔG) was computed using the NUPACK Python API^{48,49} (v4.0.1.8) with default parameters at 55°C. Nanopore basecalling was performed with Dorado⁴⁰ (v1.3.0, simplex mode) using the R10.4.1 E8.2 400 bps *fast*, *hac*, and *sup* models (v4.3.0), with a minimum Q-score threshold set to 7. Paired-end Illumina reads were merged using FLASH⁵⁰ (v1.2.11). Primer trimming and payload extraction from raw sequencing reads were performed using Cutadapt⁵¹ (v5.2), with the maximum mismatch rate set to 15%. The base-level error rates reported for the *in vitro* results were computed by aligning the reads to their corresponding reference sequences using minimap2⁵² (v2.30).

In vitro experimental workflow

Stored file and codec configurations. A compressed 24 KB text file (zlib-compressed Universal Declaration of Human Rights in four languages) was encoded using four configurations of DNA-MGC+ and one configuration each of DNA-Aeon and HEDGES. For DNA-MGC+, two parameter sets were considered, referred to as Design A and Design B. For each design, both unfiltered and filtered variants were evaluated. The corresponding number of reference sequences, payload length, and code rate are given in Table 2. Full parameter values for all evaluated codecs are provided in Supplementary Tables S1–3.

Table 2. Encoding characteristics for the considered codecs when applied to the 24-KB compressed text file.

Codec	Number of sequences	Payload length (nts)	Code rate (bits/nt)	Tag
DNA-MGC+ (Design A, filtered)	1532	124	1.03	GGAT
DNA-MGC+ (Design A, unfiltered)	1532	124	1.03	AGTG
DNA-MGC+ (Design B, filtered)	2277	122	0.71	CAAG
DNA-MGC+ (Design B, unfiltered)	2277	122	0.71	GACA
DNA-Aeon	1619	120	1.00	CTGT
HEDGES	2550	126	0.61	TAGC

Oligonucleotide design and synthesis. For each codec configuration, the encoded payload sequences were right-padded with random nucleotides to obtain a common length of 126 nts. A configuration-specific 4-nt tag was then appended to the right of each sequence (see Table 2), followed by the addition of a 20-nt forward primer AGCGTTCGTTACTTAGATAC and a 20-nt reverse primer TCACCGTATTGCGTAGTATG. The resulting sequences had a total length of 170 nt, matching the maximum length supported by the synthesis provider GenScript. A single oligo pool containing all six configurations was synthesized.

Constraint-based filtering. For the filtered DNA-MGC+ variants, an excess pool of candidate sequences was first generated using the codec. The encoded payloads were then formatted to match the 170-nt oligonucleotide structure described above, including the configuration-specific tags and primers. The sequences were subsequently screened and retained only if they satisfied the following constraints: maximum homopolymer length ≤ 4 , GC content between 45% and 55%, and absence of di- and trinucleotide repeat motifs. For the retained sequences, the folding Gibbs free energy (ΔG , in kcal/mol) was computed at 55°C, corresponding to the primer annealing temperature (T_a). Sequences with ΔG values closest to zero were preferentially selected. Histograms of the maximum homopolymer length, GC content, and ΔG for the encoded sequences of each of the six codec configurations are shown in Supplementary Fig. S3.

PCR, library preparation, and sequencing. The oligo pool from GenScript, received dry, was resuspended to a concentration of 4.5 ng μL^{-1} using nuclease-free water. For PCR amplification, 2 μL of the resuspended oligo pool (4.5 ng μL^{-1}) was mixed with 25 μL KAPA HiFi HotStart ReadyMix 2 \times (Roche), 1 μL of 10 μM forward primer, 1 μL of 10 μM reverse primer, and 21 μL nuclease-free water, yielding a final reaction volume of 50 μL . The reaction was prepared in three separate tubes. Thermocycling followed established protocols, consisting of an initial denaturation at 95°C for 5 min, followed by 30 cycles of denaturation at 95°C for 20 s, annealing at 55°C for 30 s, and extension at 72°C for 20 s. PCR products were subsequently

purified using SPRI magnetic beads (Beckman Coulter) and analyzed on a BioAnalyzer system using the High Sensitivity DNA kit and reagents (Agilent Technologies).

Libraries for Oxford Nanopore sequencing were prepared using the SQK-LSK114 ligation sequencing kit (Oxford Nanopore Technologies). Nanopore sequencing was performed on a PromethION platform using R10.4.1 PromethION flow cells. Libraries for Illumina sequencing were prepared using the NEBNext UltraExpress[®] DNA Library Prep Kit (New England Biolabs). Illumina sequencing was performed on a NextSeq 2000 system (Illumina) using a P2 flow cell and a 600-cycle kit to generate paired-end 2 × 300 bp reads. Coverage distributions derived from the Illumina and Nanopore sequencing data for each of the six codec configurations are shown in Supplementary Fig. S4.

Read processing and decoding. Raw sequencing reads were first processed to locate and trim the primer sequences and to extract the payload in between. For Illumina data, paired-end reads were merged prior to primer trimming, whereas Nanopore reads were processed directly. Reads with an extracted payload length within 10 nucleotides of the design length of 130 nts, that is between 120 and 140 nts, were retained for further analysis. The retained payload sequences were then demultiplexed into six separate files according to their configuration-specific 4-nt tags listed in Table 2. Specifically, a read was assigned to a codec configuration if the last four nucleotides of its extracted payload exactly matched the corresponding tag.

For each demultiplexed set, clustering, alignment, and consensus calling were performed. The resulting consensus sequences were directly provided to the corresponding decoder of each codec without additional processing. To determine the minimum sequencing depth required for reliable decoding, progressive downsampling was applied to the demultiplexed reads prior to clustering. For each codec configuration and each tested depth value, a number of reads equal to the product of the depth and the corresponding number of reference sequences was randomly sampled. Clustering, alignment, consensus calling, and decoding were then repeated at each depth value until the minimum depth enabling reliable decoding was identified.

Data availability

The reference sequences and the corresponding FASTQ sequencing data generated in the *in vitro* experiments are available on Zenodo at <https://doi.org/10.5281/zenodo.18848901>.

Code availability

The source code of DNA-MGC+ is publicly available at <https://github.com/ramy-khabbaz/MGCP>. The version used in this work is v1.1.

References

1. Rydning, J. Worldwide idc global datasphere forecast, 2022–2026: enterprise organizations driving most of the data growth. *Int. Data Corp. (IDC)* (2022).
2. Church, G. M., Gao, Y. & Kosuri, S. Next-generation digital information storage in DNA. *Science* **337**, 1628–1628 (2012).
3. Grass, R. N., Heckel, R., Puddu, M., Paunescu, D. & Stark, W. J. Robust chemical preservation of digital information on dna in silica with error-correcting codes. *Angewandte Chemie Int. Ed.* **54**, 2552–2555 (2015).
4. Heckel, R., Mikutis, G. & Grass, R. N. A characterization of the dna data storage channel. *Sci. reports* **9**, 9663 (2019).
5. Gimpel, A. L., Stark, W. J., Heckel, R. & Grass, R. N. A digital twin for DNA data storage based on comprehensive quantification of errors and biases. *Nat. Commun.* **14**, 6026 (2023).
6. Milenkovic, O. & Pan, C. DNA-based data storage systems: A review of implementations and code constructions. *IEEE Transactions on Commun.* **72**, 3803–3828 (2024).
7. Sabary, O., Kiah, H. M., Siegel, P. H. & Yaakobi, E. Survey for a decade of coding for DNA storage. *IEEE Transactions on Mol. Biol. Multi-Scale Commun.* **10**, 253–271 (2024).
8. Shomorony, I., Heckel, R. *et al.* Information-theoretic foundations of DNA data storage. *Foundations Trends Commun. Inf. Theory* **19**, 1–106 (2022).
9. Kas Hanna, S. On the reliability of information retrieval from MDS coded data in DNA storage. In *2025 IEEE International Symposium on Information Theory (ISIT)* (2025). Extended version available at: <https://arxiv.org/abs/2502.06618>.
10. Erlich, Y. & Zielinski, D. DNA fountain enables a robust and efficient storage architecture. *science* **355**, 950–954 (2017).
11. Gimpel, A. L., Renschak, A., Stark, W. J., Heckel, R. & Grass, R. N. Comparison of state-of-the-art error-correction coding for sequence-based DNA data storage. *bioRxiv* 2025–07 (2025).

12. Press, W. H., Hawkins, J. A., Jones Jr, S. K., Schaub, J. M. & Finkelstein, I. J. Hedges error-correcting code for DNA storage corrects indels and allows sequence constraints. *Proc. Natl. Acad. Sci.* **117**, 18489–18496 (2020).
13. Goldman, N. *et al.* Towards practical, high-capacity, low-maintenance information storage in synthesized DNA. *nature* **494**, 77–80 (2013).
14. Bornholt, J. *et al.* A DNA-based archival storage system. In *Proceedings of the twenty-first international conference on architectural support for programming languages and operating systems*, 637–649 (2016).
15. Blawat, M. *et al.* Forward error correction for DNA data storage. *Procedia Comput. Sci.* **80**, 1011–1022 (2016).
16. Organick, L. *et al.* Random access in large-scale DNA data storage. *Nat. biotechnology* **36**, 242–248 (2018).
17. Appuswamy, R. *et al.* Oligoarchive: Using DNA in the DBMS storage hierarchy. In *Biennial Conference on Innovative Data Systems Research (CIDR 2019)*, p98 (2019).
18. Chandak, S. *et al.* Improved read/write cost tradeoff in DNA-based data storage using LDPC codes. In *2019 57th Annual Allerton Conference on Communication, Control, and Computing (Allerton)*, 147–156 (IEEE, 2019).
19. Antkowiak, P. L. *et al.* Low cost DNA data storage using photolithographic synthesis and advanced information reconstruction and error correction. *Nat. communications* **11**, 5345 (2020).
20. Meiser, L. C. *et al.* Reading and writing digital data in DNA. *Nat. protocols* **15**, 86–101 (2020).
21. Lazzarotto, D. *et al.* Overview of JPEG DNA coding system for image storage on synthetic DNA. In *Applications of Digital Image Processing XLVIII* (SPIE, San Diego, United States, 2025).
22. Song, L. *et al.* Robust data storage in DNA by de bruijn graph-based de novo strand assembly. *Nat. communications* **13**, 5361 (2022).
23. Welzel, M. *et al.* DNA-Aeon provides flexible arithmetic coding for constraint adherence and error correction in DNA storage. *Nat. Commun.* **14**, 628 (2023).
24. Yan, Z., Qu, G., Chen, X., Zheng, G. & Wu, H. DNA stairloop: enabling high-fidelity data recovery and robust error correction in DNA-based data storage. *Nat. Commun.* **16**, 9191 (2025).
25. Tabatabaei Yazdi, S. H., Yuan, Y., Ma, J., Zhao, H. & Milenkovic, O. A rewritable, random-access DNA-based storage system. *Sci. reports* **5**, 14138 (2015).
26. Yazdi, S. H. T., Gabrys, R. & Milenkovic, O. Portable and error-free DNA-based data storage. *Sci. reports* **7**, 5011 (2017).
27. Ping, Z. *et al.* Towards practical and robust DNA-based data archiving using the yin–yang codec system. *Nat. Comput. Sci.* **2**, 234–242 (2022).
28. Weindel, F., Gimpel, A. L., Grass, R. N. & Heckel, R. Embracing errors can be more efficient than avoiding them through constrained coding for DNA data storage. *IEEE Transactions on Mol. Biol. Multi-Scale Commun.* **12**, 146–156, DOI: 10.1109/TMBMC.2025.3610330 (2026).
29. Anavy, L., Vaknin, I., Atar, O., Amit, R. & Yakhini, Z. Data storage in DNA with fewer synthesis cycles using composite dna letters. *Nat. biotechnology* **37**, 1229–1236 (2019).
30. Choi, Y. *et al.* High information capacity DNA-based data storage with augmented encoding characters using degenerate bases. *Sci. reports* **9**, 6582 (2019).
31. Zhao, X. *et al.* Composite hedges nanopores codec system for rapid and portable DNA data readout with high indel-correction. *Nat. Commun.* **15**, 9395 (2024).
32. Reed, I. S. & Solomon, G. Polynomial codes over certain finite fields. *J. society for industrial applied mathematics* **8**, 300–304 (1960).
33. Kas Hanna, S. Short systematic codes for correcting random edit errors in DNA storage. In *2024 IEEE International Symposium on Information Theory (ISIT)*, 663–668, DOI: 10.1109/ISIT57864.2024.10619614 (2024).
34. Khabbaz, R., Antonini, M. & Kas Hanna, S. Marker Guess & Check Plus (MGC+): An efficient short blocklength code for random edit errors. In *2025 13th International Symposium on Topics in Coding (ISTC)*, 1–5, DOI: 10.1109/ISTC65386.2025.11154528 (2025).
35. Fu, L., Niu, B., Zhu, Z., Wu, S. & Li, W. CD-HIT: accelerated for clustering the next-generation sequencing data. *Bioinformatics* **28**, 3150–3152 (2012).
36. Lassmann, T. & Sonnhammer, E. L. Kalign—an accurate and fast multiple sequence alignment algorithm. *BMC bioinformatics* **6**, 298 (2005).

37. Chen, Y.-J. *et al.* Quantifying molecular bias in DNA data storage. *Nat. communications* **11**, 3264 (2020).
38. Rashtchian, C. *et al.* Clustering billions of reads for DNA data storage. *Adv. Neural Inf. Process. Syst.* **30** (2017).
39. Edgar, R. C. Muscle5: High-accuracy alignment ensembles enable unbiased assessments of sequence homology and phylogeny. *Nat. communications* **13**, 6968 (2022).
40. Oxford Nanopore Technologies. Dorado basecalling software for oxford nanopore sequencing data. *GitHub*: <https://github.com/nanoporetech/dorado> (2025).
41. Bar-Lev, D., Sabary, O., Gabrys, R. & Yaakobi, E. Cover your bases: How to minimize the sequencing coverage in DNA storage systems. *IEEE Transactions on Inf. Theory* **71**, 192–218, DOI: 10.1109/TIT.2024.3496587 (2025).
42. Massey, J. Shift-register synthesis and bch decoding. *IEEE Transactions on Inf. Theory* **15**, 122–127, DOI: 10.1109/TIT.1969.1054260 (1969).
43. Welch, L. R. & Berlekamp, E. R. Error correction for algebraic block codes (1986). U.S. Patent 4,633,470.
44. Kas Hanna, S. GC+ code: A systematic short blocklength code for correcting random edit errors in DNA storage. *arXiv preprint, arXiv:2402.01244* (2025).
45. Sharma, P. *et al.* DNA Storage Toolkit: A modular end-to-end dna data storage codec and simulator. In *2024 IEEE International Symposium on Performance Analysis of Systems and Software (ISPASS)* (IEEE, 2024). *GitHub*: <https://github.com/prongs1996/DNAStorageToolkit>.
46. Gimpel, A. L. *et al.* dt4dds-benchmark: Benchmarking suite for DNA data storage. *GitHub*: <https://github.com/fml-ethz/dt4dds-benchmark> (2025).
47. Mateos, J., Lavenier, D., Dimopoulou, M., Genot, A. & Antonini, M. Primer design for DNA storage random access. In *CORESA 2024 - 23ème conférence sur COmpression et REprésentation des Signaux Audiovisuels*, 1–3 (Rennes, France, 2024).
48. Dirks, R. M., Bois, J. S., Schaeffer, J. M., Winfree, E. & Pierce, N. A. Thermodynamic analysis of interacting nucleic acid strands. *SIAM Rev.* **49**, 65–88, DOI: 10.1137/060651100 (2007).
49. Fornace, M. E., Porubsky, N. J. & Pierce, N. A. A unified dynamic programming framework for the analysis of interacting nucleic acid strands: Enhanced models, scalability, and speed. *ACS Synth. Biol.* **9**, 2665–2678, DOI: 10.1021/acssynbio.9b00523 (2020).
50. Magoč, T. & Salzberg, S. L. Flash: fast length adjustment of short reads to improve genome assemblies. *Bioinformatics* **27**, 2957–2963 (2011).
51. Martin, M. Cutadapt removes adapter sequences from high-throughput sequencing reads. *EMBnet. journal* **17**, 10–12 (2011).
52. Li, H. Minimap2: pairwise alignment for nucleotide sequences. *Bioinformatics* **34**, 3094–3100 (2018).

Acknowledgements

This work was supported by the France 2030 investment plan, managed by the National Research Agency (ANR), through the PEPR MolecularXiv project (ANR-22-PEXM-003) and the Initiative of Excellence Université Côte d’Azur (ANR-15-IDEX-01). The authors thank the Institute of Molecular and Cellular Pharmacology (IPMC), Sophia Antipolis, France, and its director Pascal Barbry for providing access to laboratory facilities and technical support that made the experimental work possible.

Author contributions

R.K. and S.K. designed the DNA-MGC+ codec and performed simulations and data analysis. R.K. developed the implementation code and prepared the figures and tables. S.K. wrote the manuscript, with contributions from R.K. and J.M. All authors participated in the design of the wet-lab experiment. J.M. performed the experiments and devised the thermodynamic sequence filtering procedure. M.A. and S.K. supervised the study. All authors read, revised, and approved the final manuscript.

Competing interests

The authors declare no competing interests.

Supplementary Information for: DNA-MGC+: A versatile codec for reliable and resource-efficient data storage on synthetic DNA

Ramy Khabbaz, Jérémy Mateos, Marc Antonini, and Serge Kas Hanna

Supplementary Notes

Supplementary Note S1: Detailed marker-based offset estimation for inner MGC+ code

Supplementary Note S1 extends the offset estimation framework originally introduced in Ref.³⁴, where the MGC+ code (the inner code of the DNA-MGC+ codec) was developed and analyzed in the *binary* domain. While the overall marker-based synchronization and trellis-based decoding principles remain conceptually the same, the analysis below reformulates the system in the *DNA* domain. The key differences arise from (i) base-level insertion, deletion, and substitution (IDS) errors in the underlying channel model, which modify the transition probability structure, and (ii) the explicit derivation of received DNA marker transition probabilities under quaternary alphabet statistics (Table A).

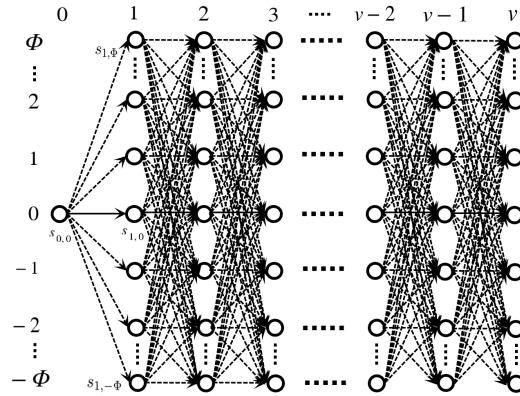


Figure A. Trellis representation of the drift sequence $\mathbf{z} = (z_0, z_1, \dots, z_v)$

Drift and Trellis Formulation For marker-based encoding, a fixed DNA marker (AC) is inserted periodically after every ℓ_{in} DNA symbols. At the decoder, synchronization is recovered by constructing a trellis whose states represent the cumulative synchronization drift after each marked block. Let the trellis state space be defined as $\Omega = \{-\Phi, -\Phi + 1, \dots, \Phi\}$, where Φ is an upper bound on the cumulative drift induced by insertion and deletion events. Let $\mathbf{z} = (z_0, z_1, \dots, z_v)$ denote the drift sequence, where $z_i \in \Omega$ is the cumulative offset after the i -th block and $z_0 = 0$. The drift evolves according to $z_i = z_{i-1} + d_i$, where d_i is the offset increment associated with block i . The received DNA sequence \mathbf{y} is segmented into blocks according to the hypothesized drift trajectory as

$$\tilde{\mathbf{b}}^{(i)} \triangleq \mathbf{y}_{[(i-1)\ell + z_{i-1} + 1, i\ell + z_i]}, \quad i \in [v], \quad (\text{S1})$$

where $\ell' = \ell + 2$. The offset increment is equivalently expressed as $d_i = z_i - z_{i-1}$. The last $\mu = 2$ nucleotides of each block correspond to the received marker sequence, denoted by $\tilde{\mathbf{m}}^{(i)}$.

Marker-centric MAP Drift Estimation Assuming independent and identically distributed IDS errors across nucleotide positions, the joint probability of observing the received sequence and a particular drift trajectory factorizes as

$$\Pr(\tilde{\mathbf{y}}, \mathbf{z}) = \prod_{i=1}^v \Pr(\tilde{\mathbf{b}}^{(i)}, z_i | z_{i-1}), \quad (\text{S2})$$

with $z_0 = 0$. To reduce decoding complexity, drift estimation is performed using only the marker observations. This leads to the following marker-centric maximum a posteriori (MAP) objective:

$$\hat{\mathbf{z}} = \arg \max_{\mathbf{z} \in \mathcal{Z}} \prod_{i=1}^v \Pr(\tilde{\mathbf{m}}^{(i)}, z_i | z_{i-1}), \quad (\text{S3})$$

where \mathcal{Z} denotes the set of all admissible trellis paths constrained to the state space Ω . A graphical illustration of the resulting trellis and its admissible transitions is provided in Fig. A.

Table A. Marker transition probabilities $\Pr(\tilde{\mathbf{m}}, D_{\text{mar}} = t)$ for the DNA marker AC.

$\tilde{\mathbf{m}}$	t	$\Pr(\tilde{\mathbf{m}}, D_{\text{mar}} = t)$
AC	0	$P_0 P_i P_d + P_r^2$
	+1	$P_r P_i + (1 - P_d - P_i) P_i P_0$
	+2	$P_i^2 P_0$
	-1	$P_0 P_r P_d + P_0^2 P_d P_s$
	-2	$P_0^2 P_d^2$
AT, AG	0	$P_s P_0 P_r$
	+1	$P_i P_0 P_s$
	-1	$2 P_d P_0^2 P_s$
	-2	$P_d^2 P_0^2$
AA	0	$P_r P_s P_0 + P_i P_d P_0$
	+1	$P_i P_s P_0$
	-1	$P_d P_0 P_r + P_0^2 P_d P_s$
	-2	$P_d^2 P_0^2$
CC, TC, GC	0	$P_0 P_s P_r + P_d P_i P_0$
	+1	$(1 - P_d - P_i) P_i P_0$
	+2	$P_i^2 P_0$
	-1	$P_0 P_r P_d + P_0^2 P_d P_s$
	-2	$P_0^2 P_d^2$
CT, CG, TT GT, GG, TG	0	$P_s^2 P_0^2$
	-1	$2 P_0^2 P_s P_d$
	-2	$P_0^2 P_d^2$
CA, TA, GA	0	$P_0 P_i P_d + P_s^2 P_0^2$
	-1	$P_0 P_r P_d + P_0^2 P_s P_d$
	-2	$P_0^2 P_d^2$

Transition Probabilities A trellis transition from state z_{i-1} to $z_i = z_{i-1} + d$ is weighted by the probability of observing a received DNA marker $\tilde{\mathbf{m}}$ together with a net offset d over the corresponding block. Since each block consists of a data segment followed by a fixed DNA marker, this probability decomposes as

$$\Pr(\tilde{\mathbf{m}}, d) = \sum_{t=-\mu}^{\mu} \Pr(D_{\text{data}} = d - t) \Pr(\tilde{\mathbf{m}}, D_{\text{mar}} = t), \quad (\text{S4})$$

where D_{data} and D_{mar} are random variables representing the cumulative offsets introduced by insertion and deletion events in the data portion and the marker portion of the block, respectively.

The data portion of each block consists of ℓ_{in} DNA nucleotides. Under the standard base-level IDS channel with deletion probability P_d , insertion probability P_i , substitution probability P_s , and $P_r = 1 - P_d - P_i - P_s$, the offset distribution $\Pr(D_{\text{data}} = t)$ depends only on the block length and channel parameters. Mathematically, it is given by

$$\Pr(D_{\text{data}} = t) = \sum_{j=\max\{0, -t\}}^{\lfloor \frac{\ell_{\text{in}} - t}{2} \rfloor} \binom{\ell_{\text{in}}}{j, j+t, \ell_{\text{in}} - 2j - t} \times P_d^j P_i^{j+t} P_r^{\ell_{\text{in}} - 2j - t}. \quad (\text{S5})$$

The marker contribution $\Pr(\tilde{\mathbf{m}}, D_{\text{mar}} = t)$ depends explicitly on the known transmitted DNA marker $\mathbf{m} = \text{AC}$, the channel parameters, and the received marker sequence $\tilde{\mathbf{m}} \in \{A, C, G, T\}^*$. Since the marker length is short ($\mu = 2$), this probability can be evaluated exactly by enumerating all possible insertion, deletion, and substitution events affecting the marker nucleotides. For completeness, Table A reports $\Pr(\tilde{\mathbf{m}}, D_{\text{mar}} = t)$ for all possible received marker sequences $\tilde{\mathbf{m}}$ and offsets $|t| \leq 2$, expressed in closed form as functions of P_d, P_i, P_s, P_r and P_0 where $P_0 = 0.25$.

Dynamic Programming Solution The MAP problem in (S3) is solved efficiently using dynamic programming. Let $\alpha_i(z_i)$ denote the maximum path metric ending at drift state z_i after processing i blocks. The recursion is

$$\alpha_i(z_i) = \max_{z_{i-1} \in \Omega} \alpha_{i-1}(z_{i-1}) \Pr(\tilde{\mathbf{m}}^{(i)}, z_i | z_{i-1}), \quad (\text{S6})$$

with initialization $\alpha_0(0) = 1$ and $\alpha_0(z) = 0$ for $z \neq 0$. The maximizing predecessor state is stored as

$$\text{pred}_i(z_i) = \arg \max_{z_{i-1} \in \Omega} \alpha_{i-1}(z_{i-1}) \Pr(\tilde{\mathbf{m}}^{(i)}, z_i | z_{i-1}). \quad (\text{S7})$$

After processing all v blocks, the estimated drift sequence $\hat{\mathbf{z}}$ is recovered by traceback starting from

$$\hat{z}_v = \arg \max_{z_v \in \Omega} \alpha_v(z_v), \quad (\text{S8})$$

and the corresponding offset pattern is obtained as $\hat{d}_i = \hat{z}_i - \hat{z}_{i-1}$, which is subsequently used for inner decoding.

Supplementary Note S2: Additional details and comments about some of the comparison codecs

LDPC Codec The LDPC-based scheme¹⁸ uses a conceptually different design from the inner–outer architectures adopted by most existing DNA storage codecs. The entire data stream is encoded using a single long binary LDPC code, whose encoded bits are then segmented into short fragments and mapped to DNA symbols. Each fragment carries a BCH-protected index and a marker to assist in handling insertions and deletions during decoding.

In our *in silico* evaluations, we used the implementation provided at https://github.com/shubhamchandak94/LDPC_DNA_Storage, keeping its default parameters and setting the `oligo_length` parameter to 150. To obtain different code rates, we replaced the underlying parity-check matrices using three matrices from https://github.com/shubhamchandak94/LDPC_DNA_storage_data/tree/master/matrices, resulting in three codec configurations with code rates of 0.58, 0.67, and 0.80 bits/nt. Among these, the configuration with rate 0.58 achieved the best overall performance under the synthetic channel model, as shown in the subsequent Supplementary Tables. However, none of the three configurations was able to decode successfully under the conditions used in the second *in silico* setting.

DNA-Stairloop The DNA-StairLoop codec²⁴ employs a concatenated coding structure consisting of a row code and a column code, but differs from the classical inner–outer architecture through the use of a staircase interleaver that couples the two component codes across adjacent blocks. Decoding follows an iterative soft-information exchange between the row and column decoders. The decoder is designed to operate directly on unclustered sequencing reads and to exploit the presence of multiple reads within its own probabilistic decoding algorithm, without relying on consensus calling. To remain consistent with the decoding procedure proposed by the authors, clustering and alignment were therefore not performed for this codec in our evaluations.

In our *in silico* experiments, we used the reference implementation available at <https://github.com/Guanjingu/StairLoop>. The parameter `msg_length` was fixed to 19 to obtain encoded DNA sequences of length 147, close to our desired target length of 150. Two values of the parameter `block_num`, 34 and 68, were used to vary the total number of encoded sequences, resulting in two codec configurations with code rates of 0.49 and 0.98 bits/nt. Our results indicate that this codec is highly sensitive to sequence dropouts under the considered parameters, leading to degraded performance under strong bias conditions. The configuration with rate 0.98 bits/nt outperformed the configuration with rate 0.49 bits/nt, suggesting that increasing the number of encoded sequences while keeping the sequence length fixed does not necessarily improve the performance of this codec. This observation is also implicit in Ref.²⁴, where the authors evaluate their codec using sequence lengths closer to 200, whereas comparison codecs are evaluated at lengths closer to 150, suggesting that DNA-Stairloop may benefit from allocating more redundancy within individual sequences, and hence operating at longer sequence lengths.

DNA-Aeon As reflected in the results in Supplementary Tables S7–S9, the decoding time of DNA-Aeon is significantly higher than that of the other codecs evaluated in this work. Decoding also becomes substantially slower at lower code rates and higher error rates. When the medium-rate configuration of DNA-Aeon was tested at an error rate of 15%, decoding ran for more than two hours without producing a result and was therefore terminated; consequently, no results are reported for this setting. The same occurred for the low-rate configuration at error rates of 10% and 15%.

Supplementary Note S3: Discussion about the effect of ΔG on the coverage distribution

As noted in the Discussion section of the main text, the modest performance improvements observed for the filtered variants of DNA-MGC+ relative to their unfiltered counterparts can be primarily attributed to the filtering criterion based on the Gibbs free energy ΔG . In particular, we observe Spearman correlation coefficients of -0.31 for Nanopore sequencing and -0.26 for Illumina sequencing between $|\Delta G|$ of unfiltered DNA-MGC+ sequences and their sequencing read counts, with p-values below 10^{-50} in both cases. These results indicate that sequences with ΔG values closer to zero tend to receive higher sequencing coverage and are therefore more likely to be decoded successfully.

This effect is further reflected in the coverage distributions shown in Supplementary Fig. S4, where the unfiltered variants consistently exhibit a substantially larger fraction of underrepresented reference sequences. For example, under Illumina sequencing for design B of DNA-MGC+, approximately 200 reference sequences in the unfiltered variant receive between 0 and 10% of the mean coverage, whereas this number decreases to roughly 50 sequences in the filtered variant. The same qualitative behavior is observed across both designs A and B and under both Illumina and Nanopore sequencing, demonstrating that filtering systematically reduces the number of poorly covered sequences.

To further investigate the origin of these underrepresented sequences, we analyzed their sequence characteristics. Under Nanopore sequencing, the subset of underrepresented reference sequences in the unfiltered variants (defined as those with read counts between 0 and 10% of the mean coverage) has an average ΔG of -6.83 kcal/mol. In contrast, the average ΔG across all reference sequences in the unfiltered variants is -4.13 kcal/mol with a standard deviation of 2.3, indicating that the underrepresented sequences are shifted by more than one standard deviation toward more negative ΔG values. This quantitative shift supports the hypothesis that sequences with more negative ΔG are less efficiently amplified or sequenced and thus receive fewer reads. By comparison, the average GC content of the underrepresented sequences is 49.9% with a standard deviation of 3.4%, suggesting that the reduced coverage of these sequences cannot be attributed to GC imbalance. Comparable trends are observed under Illumina sequencing.

A related observation emerges when comparing the two sequencing technologies. Although Illumina sequencing exhibits lower overall base-level error rates, the coverage distributions in Supplementary Fig. S4 show a larger fraction of underrepresented reference sequences compared to Nanopore sequencing. This effect is particularly pronounced for the unfiltered DNA-MGC+ variants. A plausible explanation is that Illumina sequencing relies on PCR amplification during library preparation and cluster generation, making coverage more sensitive to sequence-dependent amplification biases. In particular, the intrinsic ΔG of the sequences may influence amplification efficiency and inhibit amplification for some oligos. By contrast, this effect appears less pronounced with Nanopore sequencing, which does not rely on PCR during the sequencing process.

Supplementary Tables

Supplementary Table S1. Selected parameters for the DNA-MGC+ codec in the *in silico* and *in vitro* evaluations.

Parameter	In-silico studies				In-vitro experiment	
	Low	Medium	High	Opt	Design A	Design B
Inner Redundancy (c_{in})	12	6	0	6	6	6
Outer Redundancy (c_{out})	520	240	112	1070	306	525
Inner symbol length (ℓ_{in} , bits)	8	8	8	8	8	8
Outer symbol length (ℓ_{out} , bits)	16	16	16	16	16	16
Periodic markers	Yes	No	No	No	No	Yes
Code rate (bits/nt)	0.5	1	1.5	0.5	1.03	0.71
Sequence length (L_{ref} , nts)	152	148	152	148	124	122

Supplementary Table S2. Selected parameters for the DNA-Aeon codec used in the *in silico* and *in vitro* evaluations. These parameter settings are taken from Refs.^{11,46}.

Parameter	In-silico studies			In-vitro experiment
	Low	Medium	High	
Homopolymer	4	4	4	4
GC-content	0.0–1.0	0.0–1.0	0.0–1.0	0.0–1.0
Package redundancy	1.68	0.34	0.031	0.32
Chunk size	25	25	28	20
Sync value	4	4	8	4
Error correction	CRC	CRC	CRC	CRC
Codeword length	10	10	10	10
CRC threshold	3	3	3	3
Loop	1	1	1	1
Finish	0	0	0	0
Penalty (CRC)	0.1	0.1	0.1	0.1
Penalty (No-Hit)	8	8	8	8
Code rate (bits/nt)	0.5	1.01	1.5	1
Sequence length (nts)	149	149	144	120

Supplementary Table S3. Selected parameters for the Hedges codec used in the *in silico* and *in vitro* evaluations. The *in silico* parameter settings are taken from Refs.^{11,46}.

Parameter	In-silico studies		In-vitro experiment
	Low	Medium	
Code rate index	3	1	3
Homopolymer	4	4	4
GC window size	12	12	12
Max. GC (in window)	8	8	8
Code rate (bits/nt)	0.65	1.09	0.61
Sequence length (nts)	148	147	126

Supplementary Table S4. Selected parameters for the DNA-Fountain codec used in the *in silico* evaluations. These parameter settings are taken from Refs.^{11,46}.

Parameter	In-silico studies		
	Low	Medium	High
Alpha	2.35	0.68	0.19
Payload	32	32	34
RS length	2	2	0
Hamming distance	100	100	100
GC-content	0.0–1.0	0.0–1.0	0.0–1.0
Homopolymer	4	4	4
Delta	0.05	0.1	0.1
C-Dist	0.1	0.025	0.025
Header size	4	4	4
Code rate (bits/nt)	0.5	1	1.5
Sequence length (nts)	152	152	152

Supplementary Table S5. Minimum reliable coverage depth for different codec configurations, error rates, and bias conditions, under the synthetic channel model (in silico).

Codec	Class	Code rate	Error rate	No bias	Moderate bias	Strong bias
Aeon	Low	0.50	0.01	1.50	1.75	2.25
			0.05	5.50	8.25	15
	Medium	1.01	0.01	2.25	2.75	4.25
			0.05	4.75	8.25	10
			0.10	9.50	14.25	19.75
	High	1.50	0.01	6.25	9.25	29.50
0.05			10.75	21.25	-	
			0.10	22.25	-	-
Fountain	Medium	1	0.01	12.25	23.50	-
			0.05	25.75	-	-
	High	1.50	0.01	16	-	-
HEDGES	Low	0.65	0.01	3.25	4.75	11.50
			0.05	3.75	6.50	14
			0.10	6.25	9.25	22
			0.15	16.75	26.25	-
	Medium	1.09	0.01	3.25	4.50	11.25
			0.05	6	9	23.25
			0.10	10	16.75	-
LDPC	Low	0.58	0.01	2.75	3.25	5.75
			0.05	6.75	8.75	16.25
			0.10	18.50	24.25	-
	Low	0.67	0.01	3.50	4.50	10
			0.05	8.75	11.50	25.50
				0.10	23	32
	Medium-Low	0.80	0.01	7	11.50	-
			0.05	15.50	27.75	-
MGC+	Low	0.50	0.01	1.25	1.50	2.50
			0.05	1.75	2	3.25
			0.10	3.75	4.25	7.50
			0.15	12.50	16.25	30.25
	Medium	1	0.01	1.50	1.75	3.25
			0.05	4	5	9.25
			0.10	8.75	11.25	22.50
High	1.50	0.01	4.25	5.25	11.25	
		0.05	11.50	14.75	31.25	
RS	Low	0.50	0.01	1	1	1.25
			0.05	3.25	3.25	4.25
			0.10	8.75	8.75	10.25
	Medium	1	0.01	2.75	3	4.50
			0.05	5.50	6.50	10.25
			0.10	13.50	16	25.75
High	1.50	0.01	4.75	6.50	14.25	
		0.05	9.25	12.50	30.50	
			0.10	23	-	-
Stairloop	Low	0.49	0.01	6.25	10.25	-
			0.05	12	31	-
	Medium	0.98	0.01	5.75	12.25	-
			0.05	12.25	24	-
			0.10	30	-	-

Supplementary Table S6. Read cost (nts/bit) for different codec configurations, error rates, and bias conditions, under the synthetic channel model (in silico).

Codec	Class	Code rate	Error rate	No bias	Moderate bias	Strong bias
Aeon	Low	0.50	0.01	3	3.50	5
			0.05	11	16.50	30
	Medium	1.01	0.01	2.24	2.73	4.22
			0.05	4.72	8.20	9.94
			0.10	9.44	14.16	19.76
	High	1.50	0.01	4.15	6.15	19.60
0.05			7.14	14.12	-	
			0.10	14.78	-	-
Fountain	Medium	1	0.01	12.23	23.46	-
			0.05	25.70	-	-
	High	1.50	0.01	10.65	-	-
HEDGES	Low	0.65	0.01	4.99	7.29	17.66
			0.05	5.76	9.98	21.50
			0.10	9.60	14.20	33.78
			0.15	25.72	40.31	-
	Medium	1.09	0.01	2.97	4.12	10.30
			0.05	5.49	8.24	21.28
			0.10	9.15	15.33	-
LDPC	Low	0.58	0.01	4.71	5.57	9.85
			0.05	11.56	14.99	27.83
			0.10	31.68	41.53	-
	Low	0.67	0.01	5.20	6.68	14.84
			0.05	12.99	17.07	37.85
				0.10	34.14	47.50
	Medium-Low	0.80	0.01	8.79	14.45	-
			0.05	19.47	34.86	-
MGC+	Low	0.50	0.01	2.50	3	5
			0.05	3.50	4	6.50
			0.10	7.51	8.51	15.01
			0.15	25.02	32.52	60.54
	Medium	1	0.01	1.50	1.75	3.25
			0.05	4	5	9.26
			0.10	8.76	11.26	22.50
High	1.50	0.01	2.83	3.50	7.50	
		0.05	7.67	9.83	20.84	
RS	Low	0.50	0.01	2	2	2.50
			0.05	6.51	6.51	8.51
			0.10	17.51	17.52	20.52
	Medium	1	0.01	2.76	3.01	4.51
			0.05	5.51	6.51	10.27
			0.10	13.53	16.03	25.80
High	1.50	0.01	3.17	4.34	9.52	
		0.05	6.18	8.35	20.37	
			0.10	15.36	-	-
Stairloop	Low	0.49	0.01	12.71	20.85	-
			0.05	24.40	63	-
	Medium	0.98	0.01	5.85	12.46	-
			0.05	12.46	24.40	-
			0.10	30.51	-	-

Supplementary Table S7. Average decoding time (seconds), measured at minimum reliable coverage depth, for different codec configurations, error rates, and bias conditions, under the synthetic channel model (in silico).

Codec	Class	Code rate	Error rate	No bias	Moderate bias	Strong bias
Aeon	Low	0.50	0.01	1715.46	1427.74	1169.49
			0.05	2957.90	2423.76	3198.99
	Medium	1.01	0.01	647.93	587.18	451.27
			0.05	2223.19	1245.97	2513.76
			0.10	3236.17	3172.92	4580.02
	High	1.50	0.01	66.19	74.64	61.05
0.05			58.88	62.67	-	
0.10			1494.41	-	-	
Fountain	Medium	1	0.01	0.61	0.59	-
			0.05	0.62	-	-
	High	1.50	0.01	0.59	-	-
HEDGES	Low	0.65	0.01	10.02	7.56	6.71
			0.05	11.33	8.73	7.80
			0.10	52.70	55.27	64.61
			0.15	2248.37	2921.46	-
	Medium	1.09	0.01	5.18	5.34	4.66
			0.05	13.20	13.33	10.60
			0.10	35.01	40.12	-
LDPC	Low	0.58	0.01	164.53	161.02	155.83
			0.05	171.66	168.34	163.43
			0.10	176.77	174.87	-
	Low	0.67	0.01	138.75	147.18	141.58
			0.05	147.44	112.61	138.27
				0.10	101	129.22
	Medium-Low	0.80	0.01	123.31	131.28	-
			0.05	125.03	124.84	-
MGC+	Low	0.50	0.01	38.51	37.97	39.08
			0.05	62.64	58.18	54.74
			0.10	218.19	216.29	193.94
			0.15	3624.93	4142.30	5687.49
	Medium	1	0.01	40.88	37.56	31.34
			0.05	594.15	529.17	657.98
			0.10	1223.52	1046	1599.47
High	1.50	0.01	6.65	6.88	6.77	
		0.05	6.57	6.67	6.61	
RS	Low	0.50	0.01	2210.36	2410.36	2347.29
			0.05	2251.17	2419.03	2327.53
			0.10	2224.46	2496.38	2644.44
	Medium	1	0.01	169.56	189.42	197
			0.05	191.69	191.16	198.28
			0.10	203.49	-	205.81
High	1.50	0.01	8.20	8.16	8.48	
		0.05	8.64	9.44	7.86	
		0.10	8.64	-	-	
Stairloop	Low	0.49	0.01	606.85	1023.71	-
			0.05	1632.23	4598.35	-
	Medium	0.98	0.01	297.31	590.52	-
			0.05	882.21	1628.82	-
			0.10	2747.86	-	-

Supplementary Table S8. Performance metrics for different codec configurations under the low-fidelity experimentally derived error and bias profiles (in silico) for a fixed physical redundancy of 100×.

Codec	Class	Code rate	Sequencing depth	Read cost (nts/bit)	Avg. decoding time (s)
Aeon	Low	0.50	12.25	24.49	2440.82
	Medium	1	9.75	9.75	1533.13
HEDGES	Low	0.65	16.75	25.72	7.25
	Medium	1.09	20.25	18.53	10.65
MGC+	Low	0.50	2.50	5	41.82
	Medium	1	4.50	4.50	666.87
	Optimized	0.5	1	2	1251.82
RS	Low	0.50	3.25	6.51	2352.07
	Medium	1	12.75	12.77	210.18

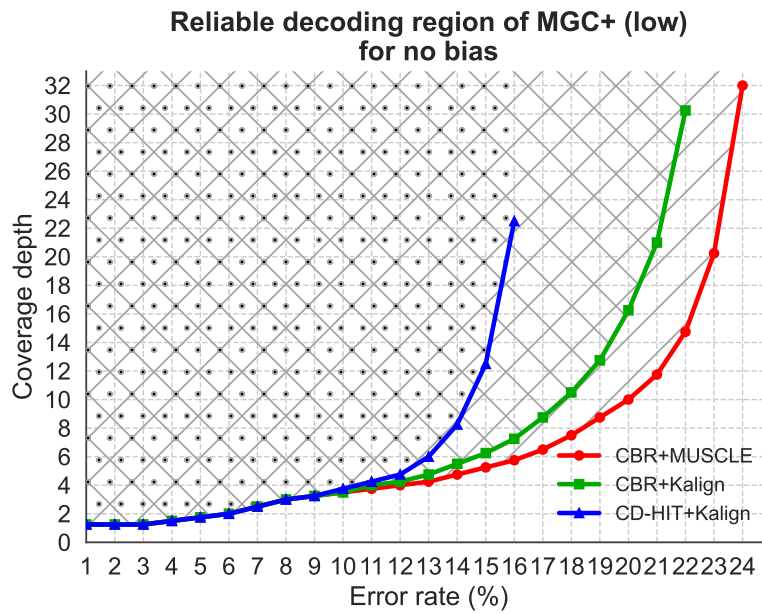
Supplementary Table S9. Performance metrics for different codec configurations under the low-fidelity experimentally derived error and bias profiles (in silico) for a fixed sequencing depth of 30×.

Codec	Class	Code rate	Physical redundancy	Write cost (nts/bit)	Avg. decoding time (s)
Aeon	Low	0.50	13.50	26.99	3223.77
	Medium	1	14.50	14.51	1584.41
HEDGES	Low	0.65	15.75	24.19	8.73
	Medium	1.09	30.75	28.14	8.12
MGC+	Low	0.50	2.25	4.50	40.78
	Medium	1	4.25	4.25	642.49
	Optimized	0.50	1	2	1190.30
RS	Low	0.50	5	10.01	2492.93
	Medium	1	20.75	20.79	214.40

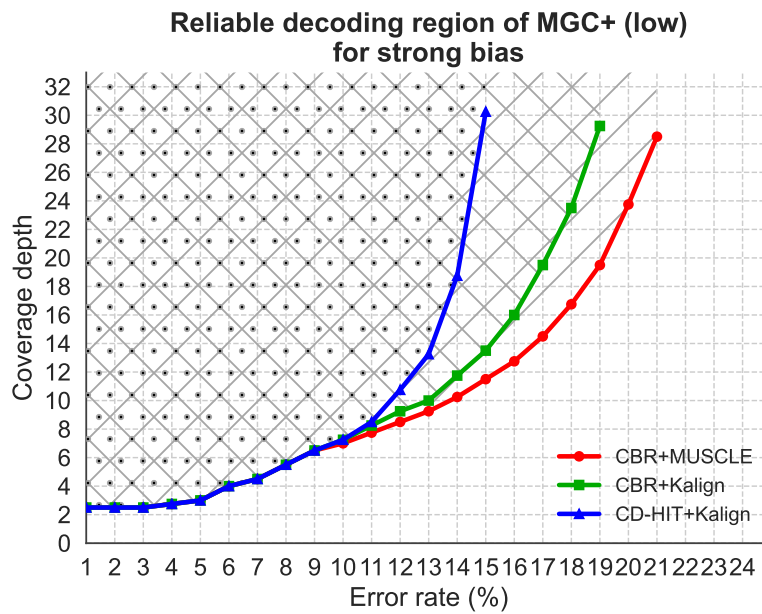
Supplementary Table S10. Minimum reliable sequencing depth, read cost, and average decoding time (serial and parallel), under Illumina sequencing and Nanopore sequencing with different basecallers (in vitro).

Sequencing method	Codec	Min. reliable sequencing depth	Code rate (bits/nt)	Read cost (nts/bit)	Avg. decoding time (s)	
					1 core	8 cores
Illumina	MGC+ (A, unfiltered)	2.75	1.032	2.66	33.34	8.08
	MGC+ (A, filtered)	2.50	1.032	2.42	207.74	13.98
	MGC+ (B, unfiltered)	2.75	0.706	3.90	58.66	7.51
	MGC+ (B, filtered)	2.25	0.706	3.19	438.83	20.09
	HEDGES	9.50	0.610	15.57	32.48	–
	Aeon	3.00	1.000	3.00	571.12	119.23
Nanopore (dorado-sup)	MGC+ (A, unfiltered)	4.00	1.032	3.88	114.65	14.53
	MGC+ (A, filtered)	3.50	1.032	3.39	193.58	22.43
	MGC+ (B, unfiltered)	3.00	0.706	4.25	63.60	7.98
	MGC+ (B, filtered)	2.75	0.706	3.90	406.03	20.89
	HEDGES	7.50	0.610	12.30	31.99	–
	Aeon	5.00	1.000	5.00	2494.72	305.97
Nanopore (dorado-hac)	MGC+ (A, unfiltered)	5.25	1.032	5.09	154.66	19.07
	MGC+ (A, filtered)	4.25	1.032	4.12	310.40	27.45
	MGC+ (B, unfiltered)	3.50	0.706	4.96	67.05	8.22
	MGC+ (B, filtered)	3.25	0.706	4.60	471.67	21.98
	HEDGES	8.25	0.610	13.52	36.28	–
	Aeon	6.50	1.000	6.50	3256.71	355.40
Nanopore (dorado-fast)	MGC+ (A, unfiltered)	10.75	1.032	10.42	389.59	40.42
	MGC+ (A, filtered)	9.25	1.032	8.96	502.40	44.36
	MGC+ (B, unfiltered)	6.75	0.706	9.56	86.09	9.76
	MGC+ (B, filtered)	6.50	0.706	9.21	503.16	23.76
	HEDGES	11.50	0.610	18.85	85.37	–
	Aeon	13.00	1.000	13.00	5071.89	537.22

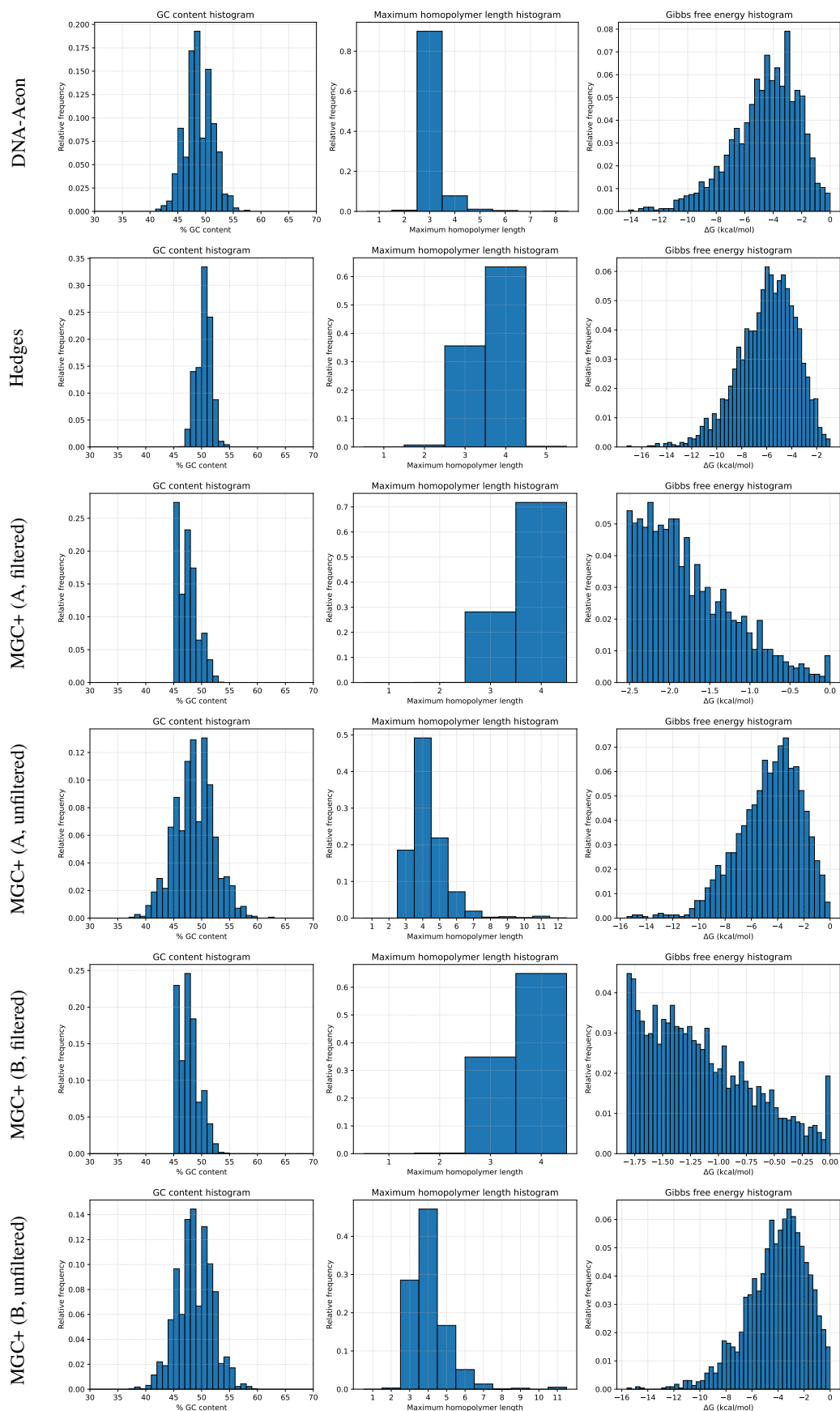
Supplementary Figures



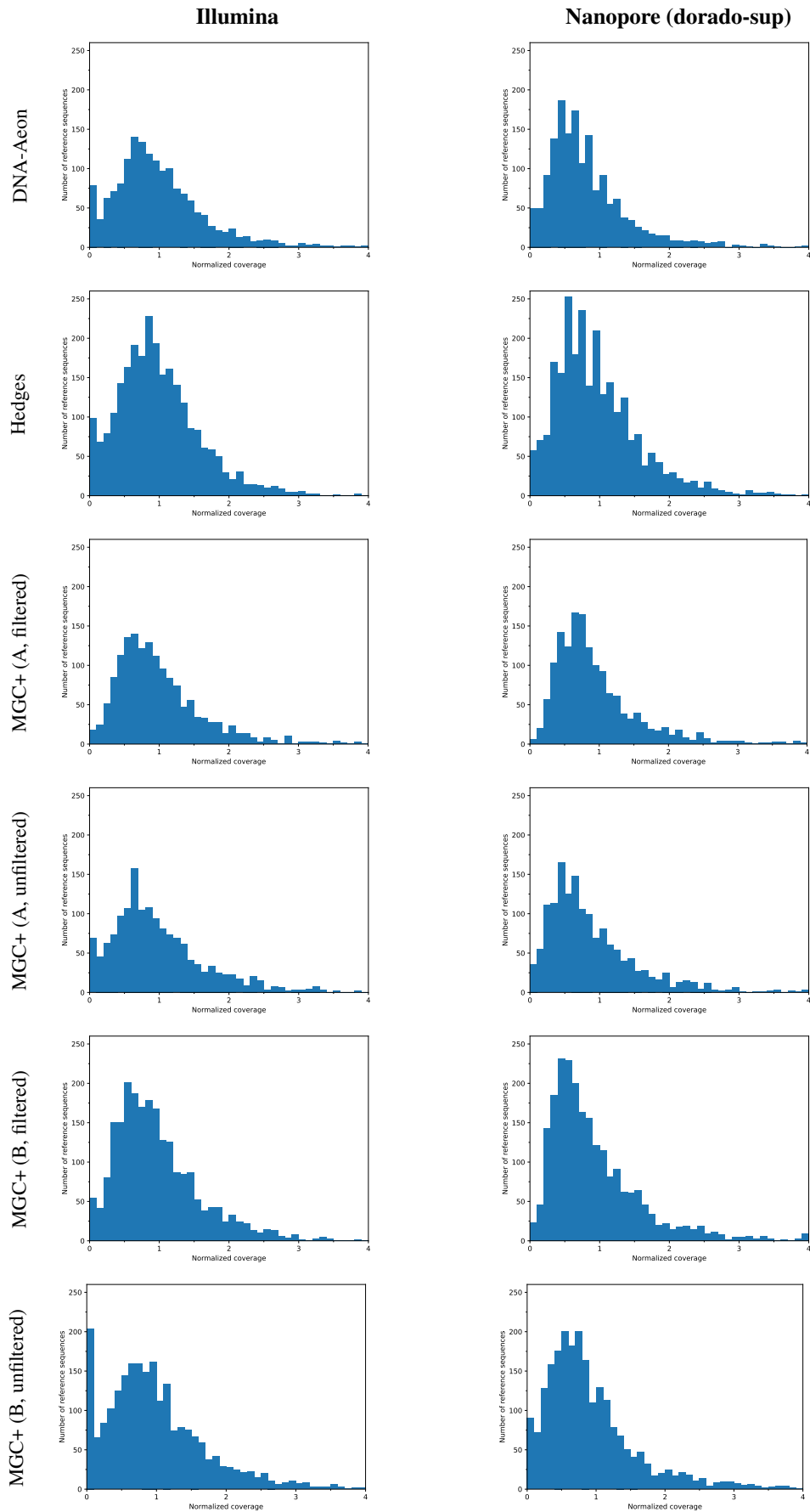
Supplementary Figure S1. Reliable decoding region of DNA-MGC+ (low-rate) for the no-bias case.



Supplementary Figure S2. Reliable decoding region of DNA-MGC+ (low-rate) for the strong-bias case.



Supplementary Figure S3. Normalized histograms of GC content, maximum homopolymer length, and Gibbs free energy (ΔG) for the encoded sequences of the different configurations included in the *in vitro* experiment.



Supplementary Figure S4. Coverage distributions derived from the Illumina and Nanopore (dorado-sup) sequencing data in the *in vitro* experiment, normalized by the mean coverage of each setting.